Cevipabulin-tubulin complex reveals a novel agent binding site on α-tubulin and provides insights into microtubule dynamic instability

Jianhong Yang[1*#], Yamei Yu[1*], Yong Li[1*], Haoyu Ye[1*], Wei Yan[1], Lu Niu[1], Yunhua Zheng[1], Zhoufeng Wang[2], Zhuang Yang[1], Heying Pei[1], Haoche Wei[1], Min Zhao[1], Jiaolin Wen[1], Linyu Yang[1], Liang Ouyang[1], Yuquan Wei[1], Qiang Chen[1], Weimin Li[2#], Lijuan Chen[1#]

[1]State Key Laboratory of Biotherapy and Cancer Center, West China Hospital of Sichuan University, Chengdu 610041, China

[2] Department of Respiratory Medicine, West China Hospital, Sichuan University, Chengdu, 610041, China

*These authors equally contribute to this work

#Correspondence should be addressed to L.C. (email: chenlijuan125@163.com) or W.L. (weimi003@scu.edu.cn) or J.Y. (yjh1988@scu.edu.cn) .

Abstract

Microtubule, composed of αβ-tubulin heterodimers, remains as one of the most popular anticancer targets for decades. To date, anti-microtubule drugs mainly target β-tubulin to inhibit microtubule dynamic instability (MDI) while agents binding to α-tubulin are less well characterized and also the molecular mechanism of MDI is far from being articulated. Cevipabulin, an oral microtubule-active antitumor clinical candidate, is widely accepted as a microtubule stabilizing agent (MSA) but binds to the microtubule -destabilization vinblastine site on β-tubulin and this unusual phenomenon has so far failed to be explained. Our X-ray crystallography study reveals that, in addition binding to the vinblastine site, cevipabulin also binds to a novel site on α-tubulin (named the seventh site) which located at the region spatially corresponding to the vinblastine site on β-tubulin. Interestingly, cevipabulin exhibits two unique site-dependent functions. Cevipabulin binding to the seventh site promotes tubulin degradation through interaction of the non-exchengeable GTP to reduce tubulin stability. Cevipabulin binding to the vinblastine site enhances longitudinal interactions but inhibits lateral interactions of tubulins, thus inducing tubulin protofilament polymerization (but not microtubule polymerization like MSAs), and then tangling into irregular tubulin aggregates. Importantly, the tubulin-cevipabulin structure is an intermediate between "bent" and "straight" tubulins and the involved bent-to-straight conformation change will be helpful to fully understand the molecular mechanism of tubulin assembly. Our findings confirm cevipabulin is not an MSA and shed light on the development of a new generation of anti-microtubule drugs targeting the novel site on α-tubulin and also

provide new insights into MDI.

Key words

Cevipabulin; Tubulin Inhibitor; Microtubule Dynamic Instability; Novel Binding Site; Tubulin Degrader.

Introduction

Microtubules play key roles in many important cell events, especially cell division, and thus remain as one of the most popular anticancer targets for decades [1, 2]. Microtubules are composed of αβ-tubulin heterodimers assembled into linear protofilaments and their packaging demands both lateral and longitudinal interactions between tubulins [3]. To date, various tubulin inhibitors have been reported to alter the lateral and/or longitudinal interactions to promote microtubule assembly or disassembly, including the clinical most popular anticancer drugs: vinca alkaloids, taxanes, eribulin *et al* [4, 5]. These drugs all target β-tubulin, which has five different binding sites (colchicine, vinblastine, paclitaxel, laulimalide and maytansine sites) [5]. By overexpression of β-tubulin isoforms, especially βIII-tubulin, cancer cells are prone to become resistant to these therapies [6]. So far, the pironetin site is the only one located on α-tubulin [5, 7]. However, this site is too small and pironetin has six chiral centers in its molecular structure, making it difficult to be synthetized. Since the crystal structure of tubulin-pironetin was reported in 2016 [5, 7], no significant progress has been made in the design of pironetin-binding-site inhibitors or even analogues of

pironetin.

Microtubule dynamic instability (MDI) is referred to the random switching between microtubule regrowth and shrinkage, which accompanied by periodic cycles of "bent" to "straight" conformation change in tubulin protofilament [8]. However, the detailed molecular mechanism of bent-to-straight conformation transition is unclear. Structural study of complexes of tubulin with the six known binding-site inhibitors allows in detail description of how inhibitors bind to and change the conformation of tubulin to alter MDI [3, 5, 9-12]. For example, inhibitors binding to paclitaxel or laulimalide site, the only two microtubule stabilization agents (MSAs) sites [13], stabilize the M-loop on β-tubulin to enhance lateral interactions to promote tubulin polymerization [9, 11], revealing a structuring of the M-loop into a short helix during tubulin polymerization [11]; Inhibitors binding to colchicine site, a widely known microtubule destabilization agents (MDAs) site [12], bind to the intra-dimer interfaces to inhibit flipping in of T7 loop on β-tubulin to inhibit tubulin polymerization [12, 14], thus demonstrating a flipping in and out of the T7 loop participating in MDI [14]. With the current existing tubulin-inhibitors complexes, some of the local conformation changes of MDI are easily observed. However, due to the lack of an intermediate structure between "bent" and "straight" of tubulin, the most important "bent" to "straight" conformation change has never been detailly described and the underlying molecular mechanism remains elusive.

Cevipabulin (or TTI-237) is a synthetic tubulin inhibitor with *in vivo* anticancer activity and has been used in clinical trials investigating the treatment of advanced

malignant solid tumors [15]. Competition experiment showed it competed with ^{3}H-vinblastine but not ^{3}H-paclitaxel for binding to microtubules, indicating it binds to the classic tubulin-depolymerization vinblastine site [16]. However, an *in vitro* tubulin polymerization assay exhibited that cevipabulin did not inhibit tubulin polymerization as vinblastine but promoted tubulin polymerization as paclitaxel [16]. These studies concluded that cevipabulin seems displaying mixed properties between paclitaxel and vinblastine. More recently, Kovalevich *et al.* identified two unusual characters of cevipabulin. Cevipabulin could promote tubulin degradation and induce lots of tubulin aggregates in cell cytoplasm which have never observed in reported known tubulin inhibitors[17]. Despite extensive efforts, the unusual phenomenon and characters of cevipabulin have so far failed to be explained and the underlying mechanism of action on microtubule has not been clearly defined [16, 18-21]. Recently, Gonzalo *et al.* synthetized an analogue of cevipabulin (named compound **2** in this paper) and got the crystal structure of tubulin-compound **2** complex (PDB code: 5NJH) and prove compound **2** binds to the vinblastine site of β-tubulin to enhance longitudinal interactions and induced formation of tubulin bundles in cell, which seems like that compound **2** binding to vinblastine site could really induce tubulin polymerization in a paclitaxel-like manner[18]. However, they didn't observe compound **2** induced microtubule through transmission electron microscope (TEM) *in vitro*, which makes their conclusion not rigorous enough.

In this study, we solved the crystal structure of tubulin-cevipabulin complex and were surprised to find that cevipabulin simultaneously binds to two spatially independent

sites: the vinblastine site and a new site on α-tubulin (called the seventh site). Detailed mechanism revealed that cevipabulin binding to the two sites exhibited two different and independent function: binding to the seventh site induces tubulin degradation and binding to vinblastine site leads to tubulin protofilament polymerization and then formation of irregular tubulin aggregates. Our study reveals that the increase in turbidity caused by cevipabulin is not the consequence of microtubule polymerization but the results of protofilament polymerization of tubulin, which well explains its paclitaxel like phenomenon but undefined function previously. Structure-activity-relationship demonstrate that trifluoropropanyl of cevipabulin plays a critical role in binding to the seventh site. Our study reveals a novel binding site on α-tubulin related to tubulin degradation effect and lays a foundation for the rational design of new generation of anticancer drugs. Importantly, we define a novel tubulin inhibition mechanism: enhancing longitudinal and inhibiting lateral interactions to induce formation of irregular tubulin aggregates and the involved bent-to-straight conformation change provides new insights into MDI.

Results

Cevipabulin induces tubulin degradation and formation of irregular tubulin aggregates

To elucidate the cellular effect of cevipabulin at an early time point, we carried out label-free quantitative proteomic analysis on six-hour cevipabulin treated human cervical adenocarcinoma cell line-HeLa. Cevipabulin significantly down-regulated the protein level of α, β-tubulin and their isoforms with high selectivity (Fig.1a). Immunoblotting study confirmed cevipabulin decreased tubulin proteins in HeLa,

human colon colorectal carcinoma cell line Hct116, human large cell lung carcinoma cell line H460 and human B cell lymphoma cell SU-DHL-6 in a dose-dependent manner (Fig.1b) and time dependent manner in HeLa cells (Fig. S1a), demonstrating that the reduction of tubulin is a common biochemical consequence of cevipabulin treatment in cancer cells. The quantitative PCR assay showed that cevipabulin had no effect on α- and β-tubulin mRNA levels (Fig.S1b), indicating that the downregulation of tubulin protein by cevipabulin is post-transcriptional. MG132, a proteasome inhibitor, could completely block cevipabulin-induced tubulin degradation (Fig.S1c). All these proved that cevipabulin promoted tubulin degradation in a proteasome dependent pathway.

Immunofluorescence staining of tubulin is commonly used to detect microtubule morphology in cells treated with tubulin inhibitors [22]. Untreated cells presented normal microtubule network in cells (Fig.1c). MSAs, such as paclitaxel, induced excessive tubulin polymerization and presented bunches of microtubules in cells (Fig.1d). MDAs, such as colchicine, inhibited tubulin polymerization and completely destroyed microtubules (Fig.1e). Vinblastine, another MDA, inhibited tubulin polymerization at low concentration (the same as colchicine, Fig. 1f), but induced the formation of tubulin paracrystals in the cytoplasm at high concentration (Fig. 1g), which was considered as packing of spiral protofilaments [3]. Interestingly, in cells treated with cevipabulin we observed a large number of irregular tubulin aggregates formation throughout the cytoplasm (Fig.1h), which was totally different from traditional MSAs and MDAs.

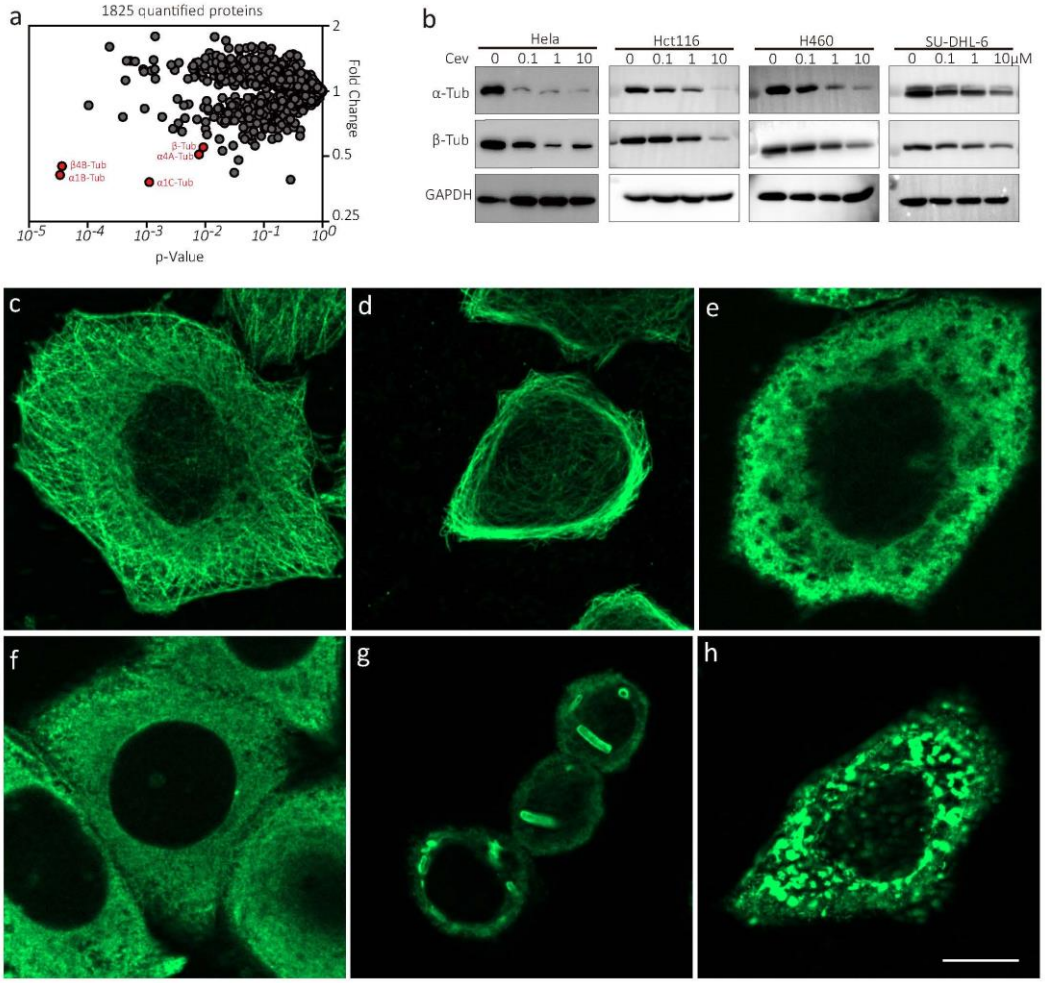

Figure 1. Cevipabulin promotes α-and β-tubulin degradation and induces the formation of irregular tubulin aggregates. (**a**) Label-free quantitative proteomic analysis of total proteins from HeLa cells treated with 1 μM cevipabulin for 6 h. This graph presents fold-changes of 1825 quantified proteins between cevipabulin and DMSO treatment groups versus the p value (t test; triplicate analysis). Three biological repetitions are performed. (**b**) Immunoblotting analysis of both α and β-tubulin levels in HeLa, Hct116, H460 and SU-DHL-6 cells, which all are treated with indicated concentrations of cevipabulin for 16 h. Results are representative of three independent experiments. (**c-h**) Hela cells are treated with (**c**) DMSO, (**d**) paclitaxel (1 μM), (**e**) colchicine (1 μM), (**f**) vinblastine (1 μM), (**g**) vinblastine (10 μM) and (**h**) cevipabulin（3 μM） for 1 hour and then subjected for immunofluorescence analysis with α-tubulin antibody to monitor morphology of microtubule. Bar=10μm. Results are representative of three independent experiments. Cev: cevipabulin.

Crystal structure of tubulin-cevipabulin reveals its simultaneously binding to the vinblastine site and a novel site on α-tubulin

To analyze the binding details of cevipabulin (Fig. 2a) to tubulin, we soaked cevipabulin

into the crystals consisting of two tubulin heterodimers, one stathmin-like protein RB3 and one tubulin tyrosine ligase (T2R-TTL) [11]. The crystal structure of tubulin-cevipabulin complex was determined to be 2.6 Å resolution (Table S1). The whole structure was identical to previously reported [11], two tubulin heterodimers were arranged in a head to tail manner (α1β1-α2β2) with the long helix RB3 comprising both dimers and tubulin tyrosine ligase docking onto α1-tubulin (Fig. 2b). The Fo–Fc difference electron density unambiguously revealed two cevipabulin molecules binding to two different sites (Fig. 2c and 2d): one at the inter-dimer interfaces between the β1- and α2-tubulin subunits (the vinblastine site) and the other one at the intra-dimer interfaces between α2- and β2-tubulin subunits (Fig. 2b) and the later binding region is a new binding site (here named as the seventh site).

The binding region of cevipabulin in the vinblastine site was formed by residues from βH6, βH7, βT5 loop, αH10 and αT7 loop (Fig.2e). As presented in Figure 2f, the side chain of βY224 made π-π stacking interactions with triazolopyrimidinyl group of cevipabulin and the guanine nucleobase of GDP (Fig.2f). Seven hydrogen bonds (N1 atom to side chain of βY224; N3 atom to main-chain nitrogen of βY224 through a water; N4 atom to main-chain nitrogen of βY224; 5- chlorine atom to both main-chain nitrogen of βY224 and βT223; 2'- fluorine atom to site chain of βY224 and main-chain nitrogen of βN206) between cevipabulin and β1-tubulin were observed. The -NH- group on the cevipabulin side chain formed a salt bridge with βD211. Besides, cevipabulin also exhibited four hydrogen bonds with α2-tubulin (oxygen atom on side chain to the side chain of αN329; 2'- fluorine atom to the main-chain nitrogen of αN326; one fluorine

187 atom of trifluoropropanyl to both main and side chain of αN326) (Fig.2g).

188 The seventh site on α2-tubulin is formed by residues from αH1, αH6, αH7, αT5, βH10
189 and βT7 (Fig.2h). Similar to the vinblastine site, triazolopyrimidinyl of cevipabulin at
190 this site also made π-π stacking interactions with the side chain of αY224 and the
191 guanine nucleobase of GTP (Fig. 2i). There were eight hydrogen bonds (N1 atom to
192 side chain of αY224; N4 atom to main-chain nitrogen of αY224; 5- chlorine atom to
193 main-chain nitrogen of αT223; 2'- fluorine atom to site chain of αN206; 6'- fluorine
194 atom to site chain of αR221; One fluorine atom of trifluoropropanyl to side chain of
195 αN206; Another fluorine atom of trifluoropropanyl to both O2' AND O3' of GTP)
196 between cevipabulin and α2-tubulin and a salt bridge between the -NH- group of
197 cevipabulin side chain and αD211 (Fig. 2i). Notably, there is no hydrogen bond between
198 cevipabulin and β2-tubulin at this new site.

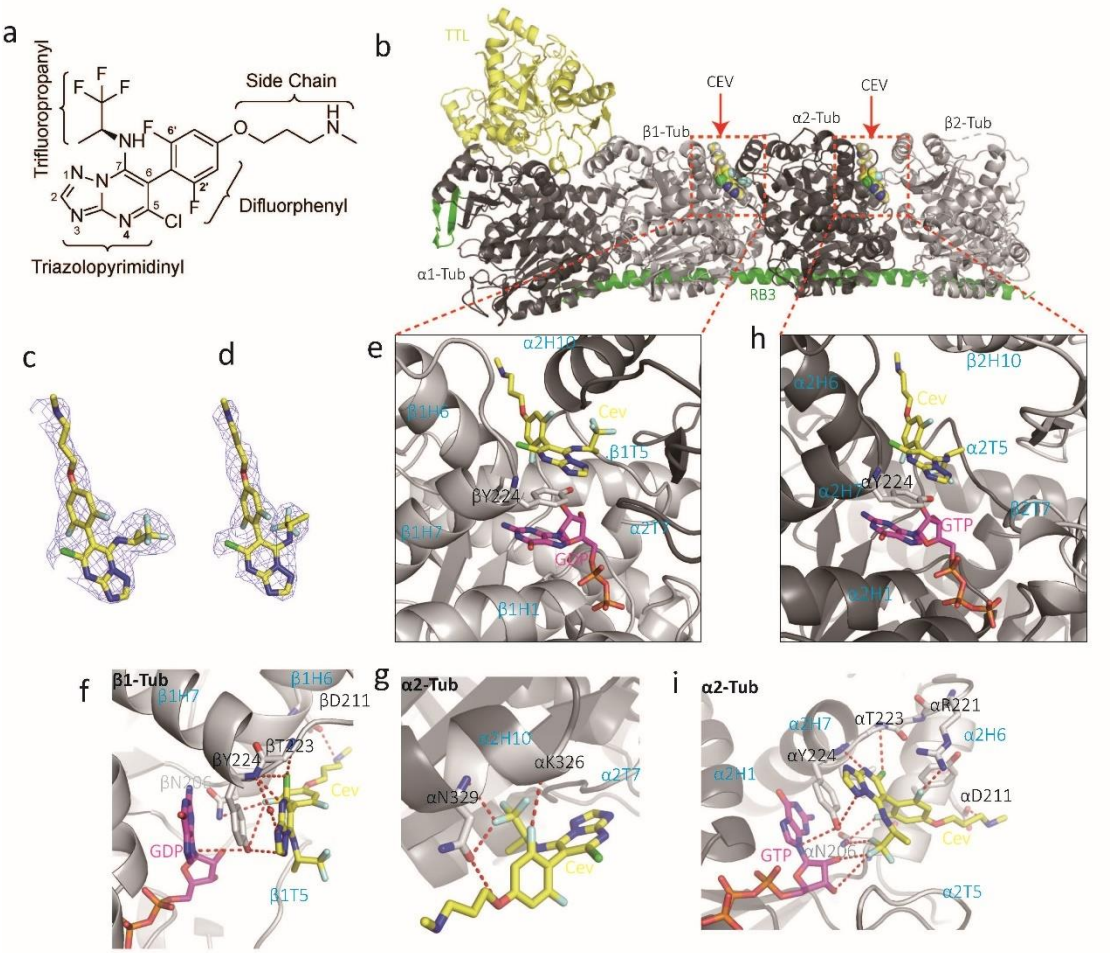

Figure 2. Crystal structure of tubulin-cevipabulin complex. (**a**) Chemical structure of cevipabulin. (**b**) Overall structure of tubulin-cevipabulin complex. TTL is colored yellow, RB3 is green, α-tubulin is dark and β-tubulin is grey. Cevipabulin on β1-tubuin and α2-tubulin are all shown in spheres and colored yellow. (**c, d**) Electron densities of cevipabulins on (**c**) β1-tubulin or (**d**) α2-tubulin. The Fo-Fc omit map is colored light blue and contoured at 3δ. (**e, f**) Close-up view of cevipabulin binding to (**e**) β1-tubulin or (**f**) α2-tubulin. GDP or GTP is shown in magenta sticks. Cevipabulin is shown in yellow sticks. Side chain of β1-Y224 or α2-Y224 is show in grey sticks. (**g, h**) Interactions between (**g**) β1-tubulinn and vinblastine-site cevipabulin or (**h**) α2-tubulin and vinblastine-site cevipabulin. Coloring is the same as in (**e**). Residues from tubulin that form interactions with vinblastine-site cevipabulin are shown as sticks and labeled. Hydrogen bonds are drawn with red dashed lines. (**i**) Interactions between α2-tubulin and the-seventh-site cevipabulin, color is the same as in (**f**), residues from tubulin that form interactions with the-seventh-site cevipabulin are shown as sticks and are labeled. Hydrogen bonds are drawn with red dashed lines. Cev: cevipabulin.

Cevipabulin binding to vinblastine site induces the formation of irregular tubulin aggregates while binding to the seventh site induces tubulin degradation

To address the functions of these two sites, we used vinblastine to block the vinblastine

site or single amino acid substitution (Y224G on α-tubulin) to block the seventh site. When vinblastine site was occupied, cevipabulin lost its ability to induce irregular tubulin aggregation, while retaining the tubulin-degradation effect (Fig. 3a and 3b). When the seventh site was mutant, cevipabulin lost the tubulin-degradation effect but persist inducing irregular tubulin aggregation (Fig. 3c and 3d). These data indicate that cevipabulin binds to the vinblastine site inducing irregular tubulin aggregation, while binds to the seventh site led to tubulin degradation.

To independently study the functions and structure activity relationship between these two sites, we employed two reported cevipabulin analogues (compounds **1 [17]** and **2 [18])** for further study **(**Fig. 3e), which only bound to the seventh site or the vinblastine site, respectively. Compared with cevipabulin, compound **1** lacks the N- substituted side chain. Further, the trifluoropropanyl in compound **1** was replaced by an azabicyclo to obtain compound **2**. We found compound **1** only induced tubulin degradation (Fig. 3f) and did not lead to irregular tubulin aggregation (Fig. 3g), in contrast, compound **2** only induced irregular tubulin aggregation but not tubulin degradation (Figs. 3f, 3g). Competition assay indicated that αY224G mutation, but neither vinblastine nor compound **2,** inhibited compound **1** induced tubulin degradation (Fig. 3h, S2a and S3b). Vinblastine, rather than compound **1** or αY224G mutation, suppressed compound **2** caused irregular tubulin aggregation (Fig. 3i, S2c and S2d). These results demonstrated that compound **1** only bond to the seventh site while compound **2** only bound to the vinblastine site, and also implied that trifluoropropanyl of cevipabulin played critical role in binding to the seventh site.

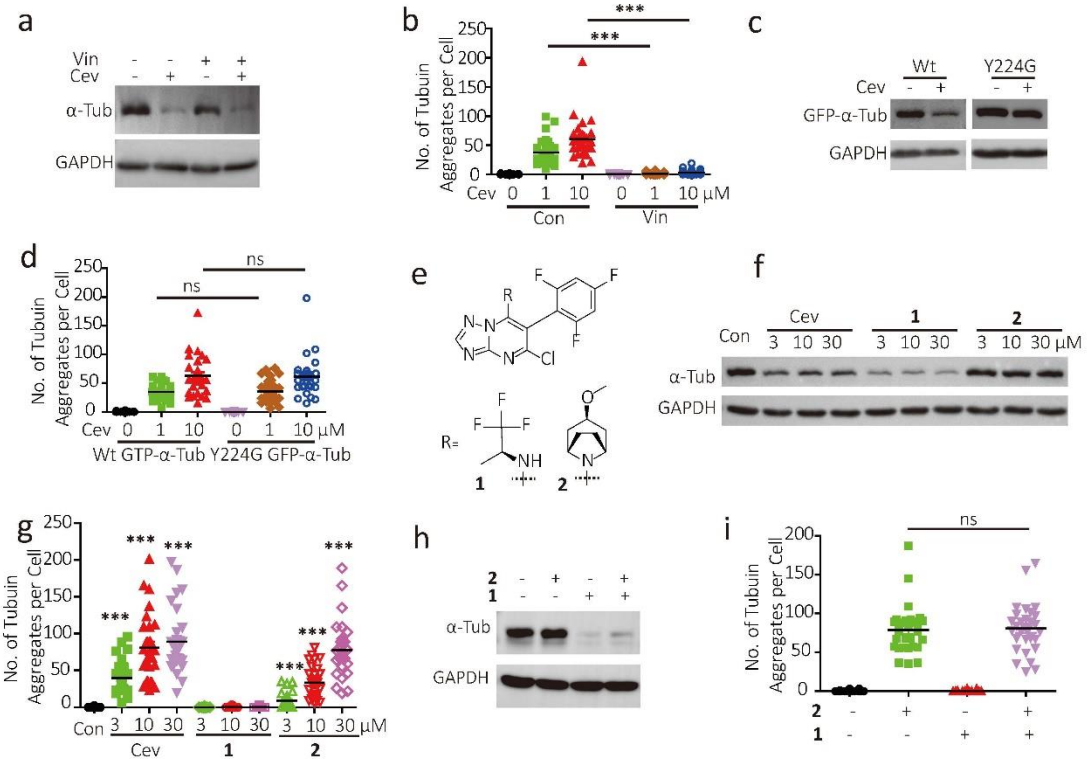

Figure 3. Cevipabulin binds to vinblastine site to induce formation of irregular tubulin aggregates while binds to the seventh site to induce tubulin degradation. (**a**) HeLa cells were treated with 10 μM vinblastine for 1 h and then further treated with 1 μM cevipabulin for 16 h. The α-tubulin protein level was detected by immunoblotting. Results are representative of three independent experiments. (**b**) HeLa cells treated with or without 10 μM vinblastine for 1 h before treated with 1 μM or 10 μM cevipabulin for another hour. Irregular tubulin aggregates were detected using immunofluorescence and the number of irregular tubulin aggregates was counted for randomly chosen 30 cells. ***p<0.00001. Results are representative of three independent experiments. (**c**) Vectors expressing either wild type or Y224G mutant GFP-tubulin were transfected to HeLa cells. After 24 hours, cells were treated with or without 1μM cevipabulin for 16 h. Then the protein level of GFP-α-tubulin was detected by immunoblotting. Results are representative of three independent experiments. (**d**) Vectors expressing either wild type or Y224G mutant GFP-α-tubulin were transfected to HeLa cells. After 24 hours, cells were treated with or without 1 μM cevipabulin for 1 h. Irregular tubulin aggregates were detected using immunofluorescence and the number of irregular tubulin aggregates was counted for randomly chosen 30 cells. ns: no significant difference. Results are representative of three independent experiments. (**e**) Chemical structure of cevipabulin derivatives. (**f**) Hela cells were treated with indicated compounds for 16 h. Then the protein level of α-tubulin was detected by immunoblotting. Results are representative of three independent experiments. (**g**) Hela cells were treated with indicated compounds for 1 h and irregular tubulin aggregates were detected using immunofluorescence and the number of irregular tubulin aggregates was counted for randomly chosen 30 cells. ns. no significant difference. ***p<0.0001 in comparison with the control. Results are representative of three independent experiments. (**h**) HeLa cells were treated with or without 30 μM compound **2** for 1 hour before treated with 10 μM compound **1** for

16 h and then the protein level of α-tubulin was detected by immunoblotting. Results are representative of three independent experiments. (**i**) HeLa cells were treated with or without 30 μM compound **1** for 1 hour before treated with 10 μM compound **2** for another hour. The irregular tubulin aggregates were detected by immunofluorescence and the number of irregular tubulin aggregates was counted for randomly chosen 30 cells. ns. no significant difference. Results are representative of three independent experiments. Cev: cevipabulin. **1**: compound **1**; **2**: compound **2**; Vin: vinblastine.

*Compound **2** promotes protofilaments polymerization by enhancing longitudinal and inhibiting lateral interactions of tubulins*

Gonzalo *et al.* reported the crystal structure of tubulin-compound **2** complex (PDB code: 5NJH) and revealed compound **2** bound to the vinblastine site can to enhance longitudinal interactions and induce the formation of tubulin bundles in cells. It seems that the binding of compound **2** to vinblastine site could induce tubulin polymerization in a paclitaxel-like manner [18]. Here we further and detailly investigated its effect on tubulin in cells. Immunofluorescence study showed that compound **2** induced short tubulin bundles (seems like microtubule bundles) formation at low concentrations (3 μM) for 1 hour treatment (Fig. 4b), which was in consistent with the published data [18]. However, when the concentration of compound **2** was increased to 10 μM, some of the tubulin bundles turned into tubulin aggregates (Fig. 4c). At higher concentration of 30 μM, the whole cytoplasm was all filled with irregular tubulin aggregates, and no tubulin bundles were observed (fig.4d), which was the same as cevipabulin treatment. Interestingly, as cells treated with 3 μM compound **2** for longer time (4h or 8h), the short tubulin bundles will also turn into irregular tubulin aggregates (Fig. 4e and 4f). To further investigate this unusual characteristic, we treated purified tubulin with compound **2** and then analyzed with TEM. As presented in Figure 4g, compound **2**

induced numbers of linear structure formation, which entangled each other to form a bundle of tubulin or tubulin aggregates. The diameter of the thinnest linear structure was about 6~7 nm (Fig. 4h), which was much smaller than that of microtubule (Fig. s3a), but perfectly matched the diameter of tubulin protofilament. These results indicated that compound **2** induced tubulin polymerizing into tubulin protofilament, but not microtubule as previously suggested [18]. Thus, it is reasonable to assume that the unusual irregular tubulin aggregates caused by compound **2** observed in cell cytoplasm are the consequence of randomly stacking and aggregation of tubulin protofilaments.

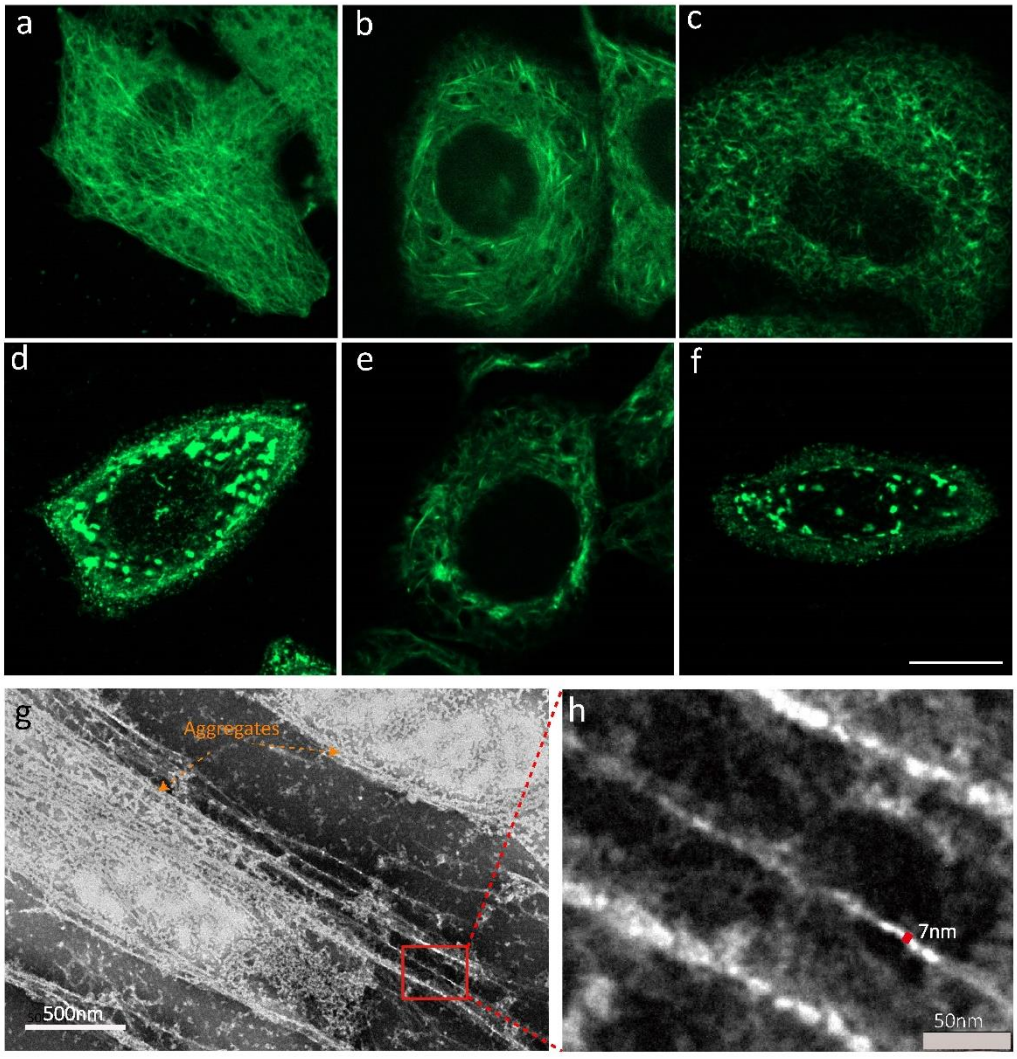

Figure 4. Compound 2 induced tubulin protofilaments polymerization. (**a-f**) Hela Cells treated with (**a**) 0, (**b**) 3, (**c**) 10 or (**d**) 30 μM compound **2** for 1 hour or treated with 3 μM compound **2** for

(**e**) 4 or (**f**) 8 h. Cells were then subjected for immunofluorescence analysis with α-tubulin antibody to monitor the morphology of microtubule. Bar=10μm. Results are representative of three independent experiments. (**g**, **h**) Purified tubulin (2mg/ml was incubated with 50 μM compound **2** for 30min at room temperature before imaged with TEM. Results are representative of three independent experiments. Both large tubulin protofilaments aggregation (**g**) and single tubulin protofilament (**h**) were observed. Results are representative of three independent experiments.

Crystal structures of tubulin-compound **2** (PDB code: 5NJH) and tubulin-cevipabulin could be superimposed very well in whole (Fig S3b, with a root-mean-square deviation (RMSD) of 0.45 Å over 1,930 Cα atoms) or in their binding region (Fig S3c). Hence, we used the tubulin-compound **2** structure for structural mechanism analysis. We superimposed the β1-tubulin subunit of tubulin-compound **2** to the one of the apo-tubulin structure (PDB code: 4I55). In the inter-dimer interfaces, compound **2** led to a 6.7 Å shift of the αH10 helix of α2-tubulin towards β1-tubulin (Fig. S3d), and thus the conformation of tubulin-compound **2** complex was arranged in a more "straight" manner than that of apo tubulin complex (Fig. S3e), implying compound **2** enhanced longitudinal interactions of tubulin dimers. We then superimposed tubulin-compound **2** complex to a polymerized microtubule structure (PDB code: 6DPV). The individual β1-tubulin or α2-tubulin in tubulin-compound **2** complex align better than those in apo tubulin structure to the corresponding subunits in polymerized microtubule structure (RMSD: 0.895 Å and 0.830 Å for β1-tubulin and α2-tubulin in tubulin-Compound **2** complex, respectively; 1.392 Å and 1.261 Å for β1-tubulin and α2-tubulin in apo tubulin, respectively), suggesting compound **2** caused both β1-tubulin or α2-tubulin to take a more "polymerized" state. Focusing on the interface of β1-tubulin and α2-tubulin, compound **2** binding caused significant movement of αT7, αH8 and αH10 to from a

depolymerized-to-polymerized state transformation (Fig. 5a and 5b). We noticed that in tubulin-compound **2** complex, the T5 loop on α2-tubulin in the intra-dimer interface showed an obvious shift from depolymerized to polymerized state (Fig.5c). As there is no ligand binding to the intra-dimer interface in the tubulin-compound **2** complex, the αT5 loop outward shift might be allosterically mediated by the inter-dimer interface conformation change. We infer that the more compact intra-dimer interface induced by compound **2** can make tubulin prone to form a straight dimer like that in the polymerized microtubule (Fig.5d), and thus straighten tubulin protofilaments. Therefore, we uncovered a continuous conformational change which could mimic the bent-to-straight conformation change during tubulin polymerization. With compound **2** binding as a small wedge, these straight protofilaments still has a 4.2° curvature at the inter-dimer interface (Fig. 5e). Also, we could clearly observe a clash between αH10 in polymerized microtubule structure and compound **2** (Fig. S3f), suggesting compound **2** binding obstructs the straight conformation of tubulins. This is in line with the fact that compound **2** can not be incorporated into polymerized microtubule [18]. To analyze the lateral interaction, we aligned tubulin-compound **2** complexes to two adjacent protofilaments in polymerized microtubule structure based on β1-tubulin. The M-loop, which is important for lateral interaction, exhibited a 5.4 Å shift between tubulin-compound **2** complex and polymerized microtubule (Fig. S3g), suggesting the M-loop is in a polymerization unfavored status. Thus, we revealed for the first time that cevipabulin or compound **2** enhanced tubulin longitudinal interactions while inhibited lateral interactions to induce excessive polymerization of tubulin protofilaments

(Fig.5f). Our results also confirm that cevipabulin is not an MSA as previously reported.

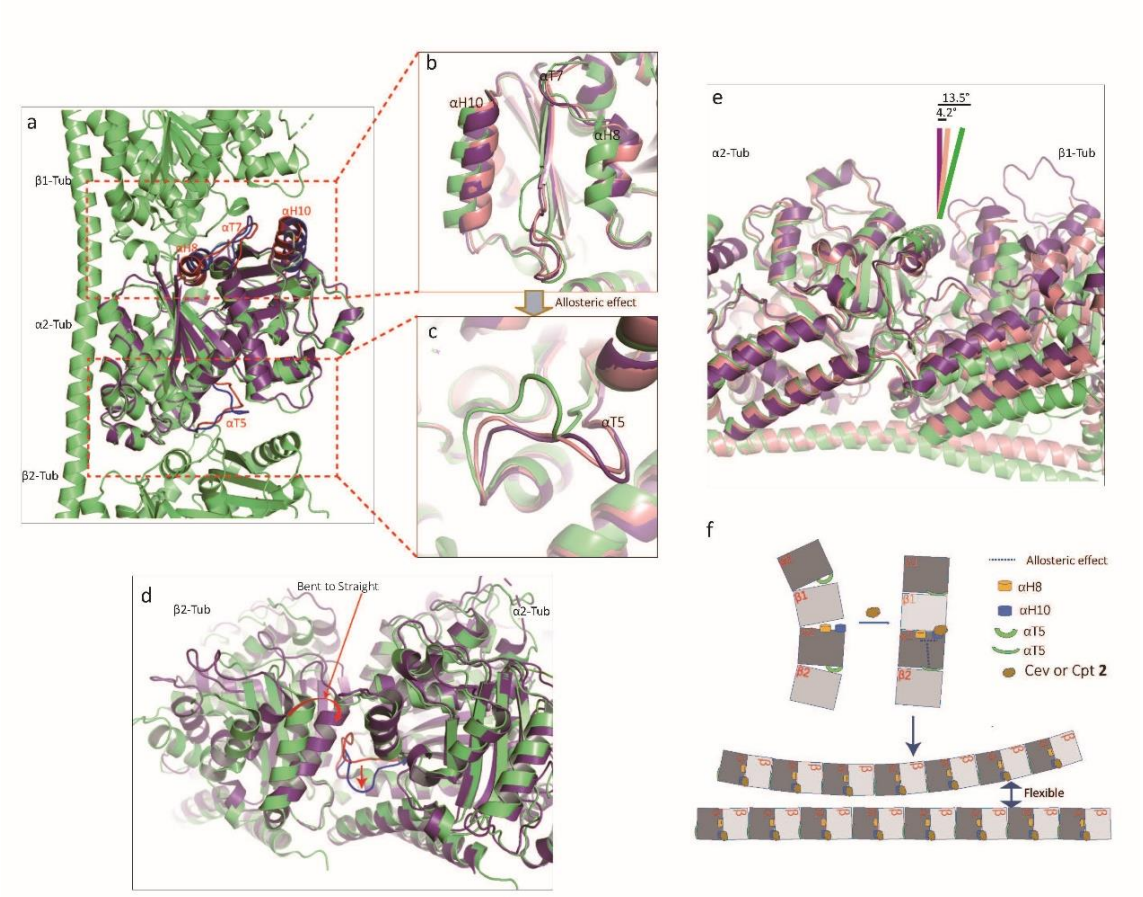

Figure 5. Structural mechanism of cevipabulin and compound 2 induced tubulin protofilaments polymerization. (**a**) Overview of the aligned structures of apo tubulin (PDB code: 4I55) and a polymerized microtubule (PDB code: 6DPV). The crystal structures of apo tubulin (green) and the polymerized microtubule (violetpurple) are superimposed on α2-tubulin subunits. β1, α2 and β2-tubulin subunits of apo tubulin structure are shown while only α2-tubulin subunit the polymerized microtubule structure is shown. αH10, αH8, αT7 and αT5 are colored blue in apo tubulin structure while red in the polymerized microtubule structure. (**b**) Tubulin-compound **2** (salmon, PDB code: 5NJH) is aligned to the superimposed complexes in (**a**) based on α2-tubulin subunit. Close-up view of the β1-α2-tubulin inter-dimer interface reveals that αH10 and αH8 in tubulin- compound **2** have a significant movement from a "depolymerized" (apo tubulin) state to a "polymerized" (polymerized microtubule structure) state. (**c**) Close-up view of the α2-β2 intra-dimer interface. The αT5 loop in tubulin-compound **2** has an outward shift to match the αT5 loop in the polymerized microtubule structure. (**d**) View of the α2, β2-tubulin interaction of the aligned complexes in (**a**). The αT5 loops of apo tubulin and microtubule are highlighted in red and blue, respectively. The αT5 loop outward shift makes room for β2-tubulin to bind closer to α2-tubulin. (**e**) View of the β1, α2-tubulin interaction of the aligned complexes in (**b**). Compared to the polymerized microtubule structure (violetpurple), The β1, α2-tubulin inter-dimer interface exhibits a 13.5° bend angle in apo tubulin structure (green) while only 4.2° in tubulin-compound **2** complex (salmon). (**f**) The molecular mechanism of cevipabulin induced tubulin protofilaments polymerization. Cev: cevipabulin. Cpt 2: compound **2.**

372 *Cevipabulin and compound **1** destabilize tubulin by interacting with the GTP on*
373 *"nonexchangeable site" to promote tubulin degradation*

374 We then investigated the tubulin degradation effect of cevipabulin binding to the
375 seventh site. At the seventh site, cevipabulin bound to the intra-dimer interface and
376 made multiple polar contacts with α2-tubulin. In particular, the trifluoropropanyl of
377 cevipabulin formed two hydrogen bonds with non-exchangeable GTP (Fig. 2i), which
378 plays a structural role and is important for the stability of tubulin dimers [23, 24]. This
379 non-exchangeable GTP forms a number of hydrogen bonds with surrounding amino
380 acid residues and a magnesian ion [23]. Single mutation abolishing hydrogen bond with
381 this GTP could reduce the affinity of GTP and absence of the magnesian ion would
382 reduce the protein stability [23, 25]. We speculated that the interaction between
383 cevipabulin and the non-exchangeable GTP could decrease tubulin stability and
384 subsequently promote tubulin degradation. Differential scanning fluorimetry (DSF) , a
385 method monitoring protein unfolding, results showed that tubulin treated by compound
386 **1** had an obvious lower Tm value (melting temperature) than DMSO treated, while
387 compound **2** increased the Tm value and cevipabulin had no significant effect on the
388 Tm value (Fig. 6a). Further the DSF results showed that compound **1** (only binds to the
389 seventh site) reduces the stability of tubulin but compound **2** (only binds the vinblastine
390 site) increases the stability of tubulin, and cevipabulin (binds to both sites) may balance
391 these two effects and represent a neutralized output. TEM results also showed that
392 compound **1** decreased tubulin stability as evidenced by lots of spherical tubulin
393 aggregates (denatured or unfolding tubulin) observed upon compound **1** treatment (Fig.

6b). Using a thiol probe, tetraphenylethene maleimide (TPE-MI), which is non-fluorescent until conjugated to a thiol [26], we further measured whether these compounds promote unfolding of tubulin. TPE-MI alone did not increase fluorescence of tubulin while addition of 4M guanidine hydrochloride (non-selective protein denaturant) significantly increased fluorescence (Fig. 6c). Cevipabulin and compound **1** obviously increased tubulin fluorescence while vinblastine and compound **2** had no such effects (Fig. 6c), demonstrating that cevipabulin or compound **1** could promote unfolding of tubulin. In addition, PYR-41, an inhibitor of ubiquitin-activating enzyme E1, totally blocked compound **1** induced tubulin degradation (Fig. 6d), suggesting destabilized tubulin is removed by normal housekeeping ubiquitinylation. Therefore, cevipabulin and compound **1** decrease tubulin stability by direct interaction with the non-exchangeable GTP to subsequently promote its destabilization and degradation.

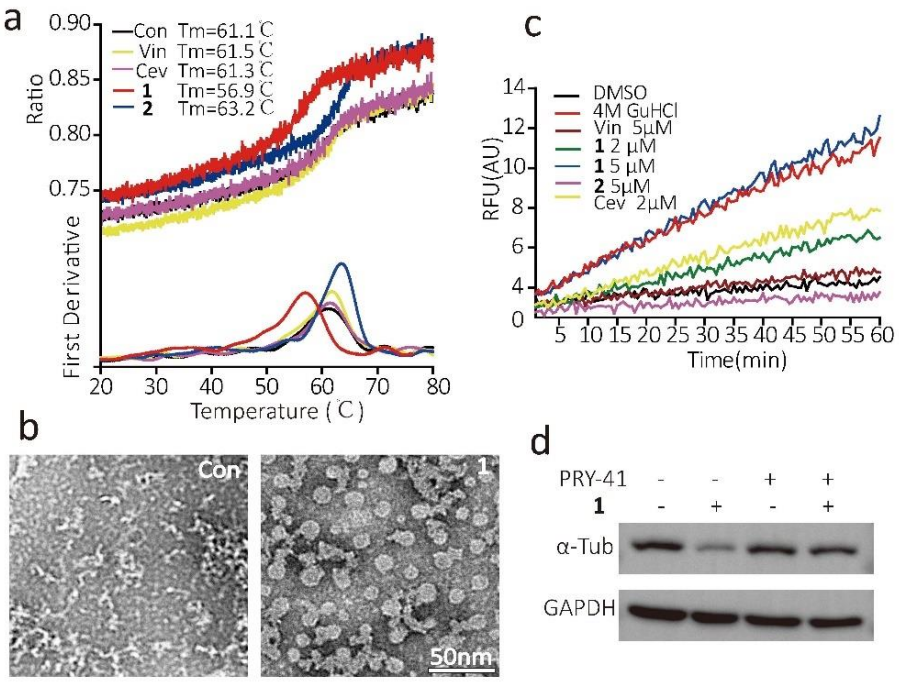

Figure 6. Cevipabulin or compound 2 decrease tubulin stability to promote tubulin destabilization and degradation. (**a**) Thermal unfolding curves of DMSO, cevipabulin (10 μM) , vinblastine (10 μM), compound **1** (10 μM) or compound **2** (10 μM) treated purified tubulin（2 μM） by a differential scanning fluorimetry (DSF) method. Plots of the fluorescence F350/F330 ratio and its first derivative are shown. The maximal values of the first derivatives are regarded as the melting temperature (Tm value). Results are representative of three independent experiments. (**b**) Purified tubulin (2mg/ml was incubated with 50 μM compound **1** for 30min at room temperature before imaged with TEM. Results are representative of three independent experiments. (**c**) Tubulin unfolding detected by TPE-MI. Tubulin (0.2 mg/ml) in PIPES buffer was mixed with 50 μM TPE-MI and the indicated compounds. Fluorescence (Excitation wavelength: 350nm; Emission wavelength: 470nm) were detected every half minute for 60 min. Results are representative of three independent experiments. (**d**) Hela cells were treated with or without PYR-41(20 μM) for 1 hour before treated with 10 μM compound **1** for 16 h. Protein level of α-tubulin were detected by immunoblotting. Results are representative of three independent experiments. Cev: cevipabulin; Vin: vinblastine. **1**: compound **1**; **2**: compound **2**.

Discussion

Our study identifies a novel binding site on α-tubulin, the seventh site. As this new site is located near the non-exchangeable GTP site and this GTP is important for tubulin stability [23-25], inhibitors such as cevipabulin and compound **1** binding to the seventh site may reduce tubulin stability and promote tubulin degradation. This novel site on α-tubulin is spatially corresponding to the vinblastine site on β-tubulin, which is also bound by cevipabulin. Cevipabulin binding to the vinblastine site enhances the longitudinal interaction within tubulin protofilaments to make them take a straighter conformation while blocks tubulin lateral interaction, causing excessive tubulin protofilaments polymerization, which randomly stack into irregular tubulin aggregates. The binding pocket of cevipabulin to these two sites is very similar (formed by αH1, αH6, αH7, αT5, βH10, βT7 for the seventh site and βH1, βH6, βH7, βT5, αH10, αT7 for the vinblastine site) and the binding modes of cevipabulin are also similar except the trifluoropropanyl of cevipabulin adopts different conformations. Vinblastine-site

cevipabulin is mainly located on β1-tubulin and makes lots of hydrogen bond with β1-tubulin while its trifluoropropanyl is oriented towards α2-tubulin and makes four hydrogen bond interactions with α2-tubulin. The-seventh-site cevipabulin is totally located on α2-tubulin and makes lots of hydrogen bond with α2-tubulin and its trifluoropropanyl is also oriented towards α2-tubulin to establish hydrogen bonds with the non-exchangeable GTP. Of note, compound **2** lacking the trifluoropropanyl could not bind to the seventh site and showed no tubulin degradation effect, suggesting the trifluoropropanyl-GTP interaction is important for cevipabulin binding to the seventh site. We noticed that in the tubulin-compound **2** complex, although compound **2** bound only to the vinblastine site, the αT5 loop at the seventh site also had an outward shift like in the tubulin-cevipabulin complex. It seems to suggest that cevipabulin binds to the vinblastine site to allosterically affect the αT5 loop with an unknown mechanism, and then creates the pocket for cevipabulin binding to α2-tubulin. However, vinblastine binding showed no such allosteric effect on αT5 loop (Fig.S3h) and can not block cevipabulin binding to the seventh site, implying cevipabulin can bind to the seventh site and affect αT5 loop itself. As compound **2** has no degradation effect but has allosteric effect on αT5 loop, we can be sure that the αT5 loop shift does not contribute to the degradation effect. Although we confirmed that compound **1** binds only to the seventh site and not to the vinblastine site, we unfortunately did not obtain the crystal structure of tubulin-compound **1** complex (possible due to compound **1**'s lower affinity to the seventh site) which might provide other vital information of the seventh site.

We confirmed that cevipabulin is not an MSA as previous reported. The previously

observed turbidity increase [16] in *in vitro* tubulin polymerization assay is likely due to tubulin protofilaments polymerization rather than microtubule polymerization. Therefore, we believe that confirmation of MSA using only in vitro tubulin polymerization assay is not rigorous. In many CNS diseases, dysregulation of microtubule structure and dynamics is commonly observed in neurons [17, 27, 28] and stabilization of microtubules by MSA is a promising therapeutic strategy [27, 29]. However, the traditional MSAs binding to the paclitaxel site have relative large molecule weights and can not penetrate the blood–brain barrier [27]. Researchers then focus on developing brain-penetrant MSAs with smaller molecule weight that could be readily synthesized, such as cevipabulin and its derivatives for the treatment of CNS diseases [30-32]. Our study indicates cevipabulin and its derivatives do not stabilize microtubule instead inversely promoting its degradation or inducing excessive tubulin protofilaments formation. These new mechanisms should be considered when studying the cevipabulin and its derivatives on CNS diseases, or there are other undiscovered mechanisms supporting their effects on CNS diseases.

Microtubules assembly demands bent-to-straight conformation change of tubulin dimers and protofilaments [8]. This conformation change is widely accepted, but the detailed molecular mechanism remains elusive. Microtubules polymerization demands GTP-bound tubulin dimers and there are two opposite models to describe the connection between GTP and tubulin dimer conformation change. The allosteric model claims that GTP binds to tubulin dimers, causing a remote allosteric conformation change to generate straighter tubulin protofilaments, and then lateral interactions

482 establishing lateral interactions to form microtubules [33-35]. However, the lattice
483 model suggests that the GTP binding has no change on tubulin dimer conformation, but
484 the lattice assembly straightens tubulin dimer to incorporate into microtubules [33, 36].
485 Since most of the evidences in support of the two models are indirect, the debates can
486 not be resolved. Here, high-resolution crystal structures of tubulin-cevipabulin and
487 tubulin-compound **2** complexes directly revealed these compounds can cause a bent-
488 to-straight conformation change in tubulin protofilament: two adjacent tubulin dimers
489 get closer, transforming the inter-dimer-interface α-tubulin into a "polymerized" state,
490 including significant movement of αH10, αH8 and αT7 in the inter-dimer interface and
491 a succedent remotely allosteric mediated αT5 outward shift in the intra-dimer interface.
492 The αT5 outward shift then makes the intra-dimer-interface β-tubulin bind to the α-
493 tubulin closer to form a straight dimer. We think this continuous conformation change
494 could reflect the bent-to-straight conformation change of tubulin dimers in normal
495 physiological condition, and provide clearly insights into MDI. More importantly, with
496 these compounds binding as a small wedge, these straight protofilaments still have a
497 4.2° curvature at the inter-dimer-interface and establish no lateral interaction,
498 demonstrating the lateral interaction requires strict straight tubulin protofilaments and
499 the lateral interaction is the consequence rather than cause of straight conformation
500 formation. Therefore, our data supports the allosteric model.
501 Here, we reported a novel binding site on α-tubulin that possessed tubulin degradation
502 effect that was distinct from the traditional MDAs and MSAs. Using this specific site,
503 a new class of tubulin degraders can be designed as anticancer drug targeting α-tubulin.

We also presented a novel function of tubulin inhibitors-induced irregular tubulin aggregation by enhancing longitudinal but blocking lateral interaction of tubulin, and the involved conformation change will provide insights into MDI.

Materials and Methods

Reagents

Colchicine, vinblastine, paclitaxel, β,γ-Methyleneadenosine 5′-triphosphate disodium salt (AMPPCP), Tetraphenylethene maleimide (TPE-MI), and DL-dithiothreitol (DTT) were purchased from Sigma; Guanidine，hydrochloride, MG132 and PYR-41 were obtained from Selleck; Cevipabulin was from MedChemExpress; Purified tubulin was bought from Cytoskeleton, Inc.; Antibodies (α-tubulin antibody, β-tubulin antibody, GAPDH antibody and gout anti mouse second antibody) were bought from Abcam.

Chemistry

All the chemical solvents and reagents used in this study were analytically pure without further purification and commercially available. TLC was performed on 0.20 mm silica gel 60 F_{254} plates (Qingdao Ocean Chemical Factory, Shandong, China). Visualization of spots on TLC plates was done by UV light. NMR data were measured for ^{1}H at 400 MHz on a Bruker Avance 400 spectrometer (Bruker Company, Germany) using tetramethylsilane (TMS) as an internal standard. Chemical shifts were quoted in parts per million. High Resolution Mass Spectra (HRMS) were recorded on a Q-TOF Bruker Daltonics model IMPACT II mass spectrometer (Micromass, Manchester, UK) in a positive mode.

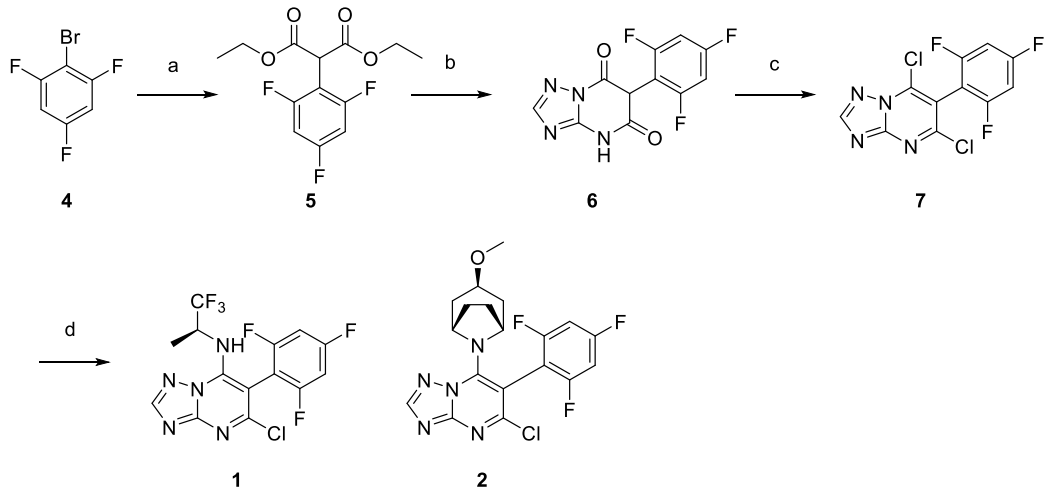

Scheme1: Reagents and conditions: a) diethyl malonate, NaH, CuI, dioxane, r.t.-reflux; b) 3-amino-1,2,4-triazole, tributylamine, 180 ℃; c) $POCl_3$, reflux; d) amine, K_2CO_3, DMF, r.t.

General procedure for the synthesis of diethyl 2-(2,4,6-trifluorophenyl)malonate (**5**)

To a stirred solution of diethyl malonate (320 mg, 2.0 mmol) in 1,4-dioxane was added 60% sodium hydride (96 mg, 2.4 mmol) by portions at room temperature. Then cupper (I) bromide (380 mg, 2.0 mmol) and compound **4** (211mg, 1.0 mmol) was added. The reaction mixture was stirred at room temperature for 30 minutes and then refluxed for 8 hours under nitrogen protection. After completion of the reaction, the mixture was cooled to room temperature and hydrochloric acid (12 N, 50 mL) was added slowly. The organic phase was separated off and the aqueous phase was extracted with ethyl acetate (×2). The combined organic phase was concentrated in vacuo. The residue was purified by chromatograph on silica gel with petroleum ether and ethyl acetate as eluent to give compound **5** as a white solid. Yield: 62%. ^{1}H NMR (400 MHz, DMSO) δ 7.36 – 7.18 (m, 2H), 5.15 (s, 1H), 4.18 (q, J = 7.1 Hz, 4H), 1.23 – 1.14 (m, 6H). HRMS-ESI: calcd for $[C_{13}H_{13}F_3O_4+Na]^+$ 313.0664, found: 313.0663.

General procedure for the synthesis of 5,7-dichloro-6-(2,4,6-trifluorophenyl)-[1,2,4]triazolo[1,5-*a*]pyrimidine (**7**)

A mixture of 3-amino-1,2,4-triazole (84 mg, 1.0 mmol), compound **5** (290 mg, 1.0 mmol) and tributylamine (1.0 mL) was heated at 180 ℃ for 4 hours. After the reaction mixture was cooled to room temperature, the residue was diluted with dichloromethane,

washed with dilute hydrochloric acid and water and crystallized from diisopropyl ether to yield 116 mg of compound **6** (brown solid, 41% yield). Then phosphorus oxitrichloride (10 mL) was added to a 25 mL round-bottom flask filled with compound **6** (282 mg, 1.0 mmol), and refluxed for 4 hours. After completion of the reaction, the reaction mixture was cooled to room temperature and the solvent was distilled off. The residue was diluted with water and ether acetate. The organic phase was separated, washed with dilute sodium bicarbonate solution and brine, dried, concentrated in vacuo and purified by chromatograph on silica gel with petroleum ether and ethyl acetate as eluent to give compound **7** as a white solid. Yield: 66%, ^{1}H NMR (400 MHz, DMSO) δ 8.90 (s, 1H), 7.62-7.55 (m, 2H). HRMS-ESI: calcd for $[C_{11}H_3Cl_2F_3N+H]^+$ 318.9765, 320.9736, found: 318.9764, 320.9739; calcd for $[C_{11}H_3Cl_2F_3N+Na]^+$ 340.9585, 342.9555, found: 340.9576, 342.9565.

General procedure for the synthesis of **1-2**

Compounds **1** and **2** were prepared as described in Zhang et al[37]. Compound **7** (160 mg, 0.5 mmol), (*S*)-1,1,1-trifluoropropan-2-amine hydrochloride (75 mg, 0.5 mmol, for **1**), or (1R,3r,5S)-3-methoxy-8-azabicyclo[3.2.1]octane (71 mg, 0.5 mmol for **2**), and potassium carbonate (276mg, 2.0 mmol) was dissolved in DMF (5 mL) and stirred at room temperature for 4 hours. After completion of the reaction, water and ethyl acetate was added. The organic phase was separated, washed with brine, dried over anhydrous sodium sulfate, concentrated in vacuo and purified by chromatograph on silica gel with petroleum ether and ethyl acetate as eluent to give compounds **1 and 2** as white solid. Yield: 48%-63%.

(S)-5-chloro-6-(2,4,6-trifluorophenyl)-N-(1,1,1-trifluoropropan-2-yl)-[1,2,4]triazolo[1,5-a]pyrimidin-7-amine (**1**)

Yield: 48%, ^{1}H NMR (400 MHz, $CDCl_3$) δ 8.40 (s, 1H), 6.93-6.89 (m, 2H), 5.96 (d, J = 10.6 Hz, 1H), 4.75 (s, 1H), 1.43 (t, J = 10.0 Hz, 3H). HRMS-ESI: calcd for $[C_{14}H_8ClF_6N_5+H]^+$ 396.0451, found 396.0488; calcd for $[C_{14}H_8ClF_6N_5+Na]^+$ 418.0270, found 418.0263.

5-chloro-7-((1*R*,3*r*,5*S*)-3-methoxy-8-azabicyclo[3.2.1]octan-8-yl)-6-(2,4,6-

trifluorophenyl)-[1,2,4]triazolo[1,5-*a*]pyrimidine (**2**)

Yield: 63%, ^{1}H NMR (400 MHz, DMSO) δ 8.57 (s, 1H), 7.52-7.48 (m, 2H), 4.58 (s, 2H), 3.43 (t, J = 4.0 Hz, 1H), 3.17 (s, 3H), 2.01 (dt, J = 10.2, 5.1 Hz, 4H), 1.90 (d, J = 14.6 Hz, 2H), 1.77 – 1.67 (m, 2H). HRMS-ESI: calcd for $[C_{19}H_{17}ClF_3N_5O+H]^+$ 424.1152, found 424.1152; calcd for $[C_{19}H_{17}ClF_3N_5O+Na]^+$ 446.0971, found 446.0964.

Cell culture

HeLa, Hct116, H460 and SU-DHL-6 cells were all sourced from American Type Culture Collection. H460 cells were cultured in RPMI 1640 medium and HeLa, Hct116 and SU-DHL-6 cells were cultured in Dulbecco's Modified Eagle's medium. Both media were supplemented with 5%-10% fetal bovine serum and about 1% penicillin-streptomycin. The culture temperature was set at 37℃, and cells were grown in a humidified incubator with 5% CO_2. All cells have been authenticated by STR tests and are free of mycoplasma.

Label free Quantitative Proteomics

HeLa cells were treated with or without 1μM cevipabulin for six hours and then all cells were collected and lysed with radioimmunoprecipitation assay buffer (containing proteinase inhibitor mixture) for 30min on ice. Then all samples were centrifuged at 10,000 g for 30 minutes to pellet cell debris. Supernatants were collected and stored at -80℃ before analysis. We have done three biological repeats. Then the following label-free quantitative proteomic analysis of these samples were carried out following the procedure as described previously[38].

Immunoblotting

Cells were plated on six-well plates and cultured for 24hours before treated with

different compounds for different time. Total cells were harvested and washed by phosphate buffer saline (PBS) before centrifuged at 1000 g for 3min. Then 1╳loading buffer (diluted from 6╳loading buffer by radioimmunoprecipitation assay buffer l) was added to the cell pellets and lysed for 10min. Samples were then incubated in boiling water for 10 min and then stored at -20℃ before use. Equal volume of samples was loaded to 10% SDS-PAGE for electrophoresis and then transferred to a polyvinylidene difluoride (PVDF) membranes at 4°C for 2 hours. Proteins on PVDF membranes were incubated in blocking buffer (5% skim milk diluted in 1╳PBST(PBS buffer with 0.1% Tween-20)) for 1hours. Then the PVDF membranes were incubated with first antibodies (diluted in blocking buffer) for 12hours and washed for three times with PBST before incubated with second antibody (diluted in blocking buffer) for 45 min and washed for three times with PBST again. At last, the PVDF membranes were immersed in enhanced chemiluminescence reagents for 30 seconds subjected to image with a chemiluminescence image analysis system (Tianneng, China).

Immunofluorescence

HeLa cells were grown on microscope cover glass in 24-well plates for 24 hours before treated with different compounds for various time. Then the medium was removed and cells were washed with prewarmed (37℃) PBS for 2 min before fixed with 50% methanol/ 50% acetone for 3 min. The fixed cells were washed with PBS for 2 min again before incubated with α-tubulin antibody (dilute in PBST containing 5% bovine serum albumin) for 4 h at room temperature. Cells were then washed with PBST for tree times (3╳5 min) and followed by incubation in fluorescent second antibody (dilute

in PBST containing 5% bovine serum albumin) for 45min at room temperature. Three times wash with PBST was performed again to remove unbounded second-antibody before imaging using a fluorescence microscope (Zeiss, Germany)

Quantitative-PCR

HeLa and Hct116 cells were plated on six-well plates and culture for 24hours before treated with cevipabulin for different time. Total mRNA of both HeLa and Hct116 cells were extracted with TRIzol (Invitrogen, USA) agents following the manufacturer's protocol and then qualified using a NanoDrop1000 spectrophotometer (Thermo Fisher Scientific, USA. The cDNA synthesis was carried out using a high Capacity cDNA Reverse Transcription Kit (Applied Biosystems, USA). Taq Universal SYBR Green Supermix (BIO-RAD, USA) was employed for further Quantitative PCR analysis on a CFX96 Real-time PCR System (BIO-RAD, USA). Relative mRNA level of both *α-tubulin* and *β-tubulin* were normalized to that of GAPDH.

Single amino acid substitution on α-tubulin

The pIRESneo-EGFP-alpha Tubulin plasmid was obtained from Addgene (USA) and mutation (Y224G) of α-Tubulin were performed using a Q5 Site-Directed Mutagenesis kit (NEB #E0554S, USA). Hela cells were plated on six-well plates and incubated for 24 hours before transfected with these plasmids by Lipofectamine 2000. Then cells were culture for another 24hours before treated with or without different compounds for 16hours. Total protein was extracted and analyzed by immunoblotting to detect the content of GTP-α-tubulin and GAPDH was employed as loading control.

Transmission electron microscopy

Purified porcine tubulin (2mg/ml) was diluted in PIPES buffer (80 mM PIPES, pH 6.9, 0.5 mM EGTA, 2 mM $MgCl_2$) supplemented with 1 mM GTP. Different compounds were then incubated with tubulin at room temperature for 30 min. About 5μL of each sample solution was added to a 230-mesh per inch, carbon films supported formvar. Then the sample was stained with 2% (w/v) phosphotungstic acid for 60 seconds. A Tecnai G2 F20 S-TWIN electron microscope (FEI, USA) was used for observation.

Differential Scanning Fluorimetry

Purified porcine tubulin (0.2mg/ml) was diluted in PIPES buffer supplemented with 1 mM GTP. Different compounds were added to tubulin solution and incubated for15min at room temperature. Then capillaries were immersed into tubulin solutions to load the samples for tests using the nanoDSF (Prometheus NT.48, NanoTemper, Germany). The temperature range was set at 20-80℃ and heating rate at 1℃/min. The fluorescence of tryptophan fluorescence at 330nm (330F) and 350nm (350F) were detected and the melting temperatures (Tm value) of tubulin were calculated as the maximum of the first derivative of the F350/F330 fluorescence ratios.

TPE-MI as a thiol probe to detect unfolded protein

TPE-MI is a small molecule which is inherently non-fluorescent until covalently binds to a thiol by its maleimide [26, 39]. This molecule could be used to monitor purified protein unfolding *in vitro* [26]. Purified tubulin (0.2mg/ml) was diluted in PIPES buffer supplemented with 1 mM GTP and then mixed with 50 μM TPE-MI and different compounds. The samples were then immediately subjected to a microplate reader (Biotek, USA) to detect the fluorescence (Excitation wavelength:350nm; Emission

wavelength: 470nm) every half minute for 60 min.

Structural Biology

Protein expression and purification were detailly described in our precious study [40]. Tubulin, RB3 and TTL (2:1.3:1.2 molar ratio) were mixed together, then 5 mM tyrosine, 10 mM DTT and 1 mM AMPPCP were added and then the mixture was concentrated to about 15 mg/ml at 4 ℃. The crystallization is conducted using a sitting-drop vapor-diffusion method under 20℃ and the crystallization buffer is optimized as: 6% PEG4000, 8% glycerol, 0.1 M MES (pH 6.7), 30 mM $CaCl_2$, and 30 mM $MgCl_2$. Seeding method was also used to obtain single crystals. Crystals appeared in about 2-days and in a rod like shape and the size reached maximum dimensions within one week. About 0.1 μL cevipabulin (diluted in DMSO with a concentration of 100 mM) was added to a drop containing tubulin crystal and incubated for 16 h at 20 ℃. The following data collection and structure determination were the same as previous description [40].

Statistical analysis

Data are presented as means. Statistical differences were determined using an unpaired Student's t test. p values are indicated in figure legend when necessary: **, $p< 0.001$; ***, $p< 0.0001$.

Acknowledgement

This work received funds from National Natural Science Foundation of China (81872900, 81803021); 1.3.5 project for disciplines of excellence, West China Hospital, Sichuan University; National Major Scientific and Technological Special Project for 'Significant New Drugs Development' (2018ZX09201018-021); Post-Doctor Research

687 Project, Sichuan University (2020SCU12036); China Postdoctoral Science Foundation
688 Grants (2019T120855 and 2019M650248); Sichuan Science and Technology Program
689 Grants (2019YJ0088, 2019YFH0123 and 2019YFH0124). Post-doctoral Research
690 Project, West China Hospital, Sichuan University Grant 2018HXBH027.

691 **Author contributions**

692 J.Y. performed most of the cellular and biochemical experiments and wrote the draft.
693 J.Y., Y.Y., W.Y, L.N. and Q.C. performed the structural biology experiments. Y.L.
694 synthesized all chemical compounds. H.Y., Y.Z., Z.W., Z.Y., H.P., H.W., M.Z., J. W.
695 L.Y., and L.O., performed some of these biochemical experiments. W.Y., J.Y., W.L. and
696 L.C. conceived the idea and supervised the study. J.Y., Q.C., W.L. and L.C. revised the
697 manuscript.

698 All authors approved the final manuscript.

699 **Conflict of interest**

700 The authors declare no competing financial interests.

701 **Data availability.**

702 Atomic coordinates and structure factors of tubulin complexed with cevipabulin have
703 been deposited in the Protein Data Bank under accession code 7CLD. Further
704 information and requests for resources and reagents should be directed to and will be
705 fulfilled by Jianhong Yang (yjh1988@scu.edu.cn).

706 **Reference**

707 [1] Arnst KE, Banerjee S, Chen H, Deng S, Hwang DJ, Li W, et al. Current advances of tubulin
708 inhibitors as dual acting small molecules for cancer therapy. Medicinal research reviews.
709 2019;39:1398-426.
710 [2] Haider K, Rahaman S, Yar MS, Kamal A. Tubulin inhibitors as novel anticancer agents: an

711 overview on patents (2013-2018). Expert opinion on therapeutic patents. 2019;29:623-41.
712 [3] Gigant B, Wang C, Ravelli RB, Roussi F, Steinmetz MO, Curmi PA, et al. Structural basis for the
713 regulation of tubulin by vinblastine. Nature. 2005;435:519-22.
714 [4] Doodhi H, Prota AE, Rodríguez-García R, Xiao H, Custar DW, Bargsten K, et al. Termination of
715 protofilament elongation by eribulin induces lattice defects that promote microtubule
716 catastrophes. Current Biology. 2016;26:1713-21.
717 [5] Yang J, Wang Y, Wang T, Jiang J, Botting CH, Liu H, et al. Pironetin reacts covalently with
718 cysteine-316 of α-tubulin to destabilize microtubule. Nature communications. 2016;7:1-9.
719 [6] Kavallaris M. Microtubules and resistance to tubulin-binding agents. Nature Reviews Cancer.
720 2010;10:194-204.
721 [7] Prota AE, Setter J, Waight AB, Bargsten K, Murga J, Diaz JF, et al. Pironetin binds covalently to
722 αCys316 and perturbs a major loop and helix of α-tubulin to inhibit microtubule formation. Journal
723 of Molecular Biology. 2016;428:2981-8.
724 [8] Manka SW, Moores CA. The role of tubulin–tubulin lattice contacts in the mechanism of
725 microtubule dynamic instability. Nature structural & molecular biology. 2018;25:607-15.
726 [9] Prota AE, Bargsten K, Northcote PT, Marsh M, Altmann KH, Miller JH, et al. Structural basis of
727 microtubule stabilization by laulimalide and peloruside A. Angewandte Chemie International
728 Edition. 2014;53:1621-5.
729 [10] Prota AE, Bargsten K, Diaz JF, Marsh M, Cuevas C, Liniger M, et al. A new tubulin-binding site
730 and pharmacophore for microtubule-destabilizing anticancer drugs. Proceedings of the National
731 Academy of Sciences. 2014;111:13817-21.
732 [11] Prota AE, Bargsten K, Zurwerra D, Field JJ, Díaz JF, Altmann K-H, et al. Molecular mechanism
733 of action of microtubule-stabilizing anticancer agents. Science. 2013;339:587-90.
734 [12] Ravelli RB, Gigant B, Curmi PA, Jourdain I, Lachkar S, Sobel A, et al. Insight into tubulin
735 regulation from a complex with colchicine and a stathmin-like domain. Nature. 2004;428:198-202.
736 [13] Steinmetz MO, Prota AE. Microtubule-targeting agents: strategies to hijack the cytoskeleton.
737 Trends in cell biology. 2018;28:776-92.
738 [14] Dorléans A, Gigant B, Ravelli RB, Mailliet P, Mikol V, Knossow M. Variations in the colchicine-
739 binding domain provide insight into the structural switch of tubulin. Proceedings of the National
740 Academy of Sciences. 2009;106:13775-9.
741 [15] Ayral-Kaloustian S, Zhang N, Beyer C. Cevipabulin (TTI-237): preclinical and clinical results for
742 a novel antimicrotubule agent. Methods and findings in experimental and clinical pharmacology.
743 2009;31:443.
744 [16] Beyer CF, Zhang N, Hernandez R, Vitale D, Lucas J, Nguyen T, et al. TTI-237: a novel
745 microtubule-active compound with in vivo antitumor activity. Cancer research. 2008;68:2292-300.
746 [17] Kovalevich J, Cornec A-S, Yao Y, James M, Crowe A, Lee VM-Y, et al. Characterization of brain-
747 penetrant pyrimidine-containing molecules with differential microtubule-stabilizing activities
748 developed as potential therapeutic agents for Alzheimer's disease and related tauopathies. Journal
749 of Pharmacology and Experimental Therapeutics. 2016;357:432-50.
750 [18] Sáez-Calvo G, Sharma A, de Asís Balaguer F, Barasoain I, Rodríguez-Salarichs J, Olieric N, et
751 al. Triazolopyrimidines are microtubule-stabilizing agents that bind the Vinca inhibitor site of
752 tubulin. Cell chemical biology. 2017;24:737-50. e6.
753 [19] Nasrin SR, Kabir AMR, Konagaya A, Ishihara T, Sada K, Kakugo A. Stabilization of microtubules
754 by cevipabulin. Biochemical and biophysical research communications. 2019;516:760-4.

[20] Nasrin SR, Ishihara T, Kabir AMR, Konagaya A, Sada K, Kakugo A. Comparison of microtubules stabilized with the anticancer drugs cevipabulin and paclitaxel. Polymer Journal. 2020:1-8.

[21] Beyer CF, Zhang N, Hernandez R, Vitale D, Nguyen T, Ayral-Kaloustian S, et al. The microtubule-active antitumor compound TTI-237 has both paclitaxel-like and vincristine-like properties. Cancer chemotherapy and pharmacology. 2009;64:681-9.

[22] Stanton RA, Gernert KM, Nettles JH, Aneja R. Drugs that target dynamic microtubules: a new molecular perspective. Medicinal research reviews. 2011;31:443-81.

[23] Menéndez M, Rivas G, Dı´az JF, Andreu JM. Control of the structural stability of the tubulin dimer by one high affinity bound magnesium ion at nucleotide N-site. Journal of Biological Chemistry. 1998;273:167-76.

[24] Spiegelman BM, Penningroth SM, Kirschner MW. Turnover of tubulin and the N site GTP in Chinese hamster ovary cells. Cell. 1977;12:587-600.

[25] Keays DA, Tian G, Poirier K, Huang G-J, Siebold C, Cleak J, et al. Mutations in α-tubulin cause abnormal neuronal migration in mice and lissencephaly in humans. Cell. 2007;128:45-57.

[26] Chen MZ, Moily NS, Bridgford JL, Wood RJ, Radwan M, Smith TA, et al. A thiol probe for measuring unfolded protein load and proteostasis in cells. Nature communications. 2017;8:1-11.

[27] Zhang B, Maiti A, Shively S, Lakhani F, McDonald-Jones G, Bruce J, et al. Microtubule-binding drugs offset tau sequestration by stabilizing microtubules and reversing fast axonal transport deficits in a tauopathy model. Proceedings of the National Academy of Sciences. 2005;102:227-31.

[28] Zhang F, Su B, Wang C, Siedlak SL, Mondragon-Rodriguez S, Lee H-g, et al. Posttranslational modifications of α-tubulin in alzheimer disease. Translational neurodegeneration. 2015;4:1-9.

[29] Zhang B, Carroll J, Trojanowski JQ, Yao Y, Iba M, Potuzak JS, et al. The microtubule-stabilizing agent, epothilone D, reduces axonal dysfunction, neurotoxicity, cognitive deficits, and Alzheimer-like pathology in an interventional study with aged tau transgenic mice. Journal of Neuroscience. 2012;32:3601-11.

[30] Ballatore C, Brunden KR, Trojanowski JQ, Lee VM-Y, Smith III AB. Non-naturally occurring small molecule microtubule-stabilizing agents: A potential tactic for CNS-directed therapies. ACS Publications; 2017.

[31] Lou K, Yao Y, Hoye AT, James MJ, Cornec A-S, Hyde E, et al. Brain-penetrant, orally bioavailable microtubule-stabilizing small molecules are potential candidate therapeutics for Alzheimer's disease and related tauopathies. Journal of medicinal chemistry. 2014;57:6116-27.

[32] Brunden KR, Trojanowski JQ, Smith III AB, Lee VM-Y, Ballatore C. Microtubule-stabilizing agents as potential therapeutics for neurodegenerative disease. Bioorganic & medicinal chemistry. 2014;22:5040-9.

[33] Rice LM, Montabana EA, Agard DA. The lattice as allosteric effector: structural studies of αβ- and γ-tubulin clarify the role of GTP in microtubule assembly. Proceedings of the National Academy of Sciences. 2008;105:5378-83.

[34] Nogales E, Wang HW. Structural mechanisms underlying nucleotide-dependent self-assembly of tubulin and its relatives. Current Opinion in Structural Biology. 2006;16:221-9.

[35] Wang H-W, Nogales E. Nucleotide-dependent bending flexibility of tubulin regulates microtubule assembly. Nature. 2005;435:911-5.

[36] Buey RM, Díaz JF, Andreu JM. The nucleotide switch of tubulin and microtubule assembly: a polymerization-driven structural change. Biochemistry. 2006;45:5933-8.

[37] Zhang N, Ayral-Kaloustian S, Nguyen T, Afragola J, Hernandez R, Lucas J, et al. Synthesis and SAR of [1, 2, 4] triazolo [1, 5-a] pyrimidines, a class of anticancer agents with a unique mechanism of tubulin inhibition. Journal of medicinal chemistry. 2007;50:319-27.

[38] Yang J, Li Y, Yan W, Li W, Qiu Q, Ye H, et al. Covalent modification of Cys-239 in β-tubulin by small molecules as a strategy to promote tubulin heterodimer degradation. Journal of Biological Chemistry. 2019;294:8161-70.

[39] Liu Y, Yu Y, Lam JW, Hong Y, Faisal M, Yuan WZ, et al. Simple Biosensor with High Selectivity and Sensitivity: Thiol-Specific Biomolecular Probing and Intracellular Imaging by AIE Fluorogen on a TLC Plate through a Thiol–Ene Click Mechanism. Chemistry–A European Journal. 2010;16:8433-8.

[40] Niu L, Yang J, Yan W, Yu Y, Zheng Y, Ye H, et al. Reversible binding of the anticancer drug KXO1 (tirbanibulin) to the colchicine-binding site of β-tubulin explains KXO1's low clinical toxicity. Journal of Biological Chemistry. 2019;294:18099-108.

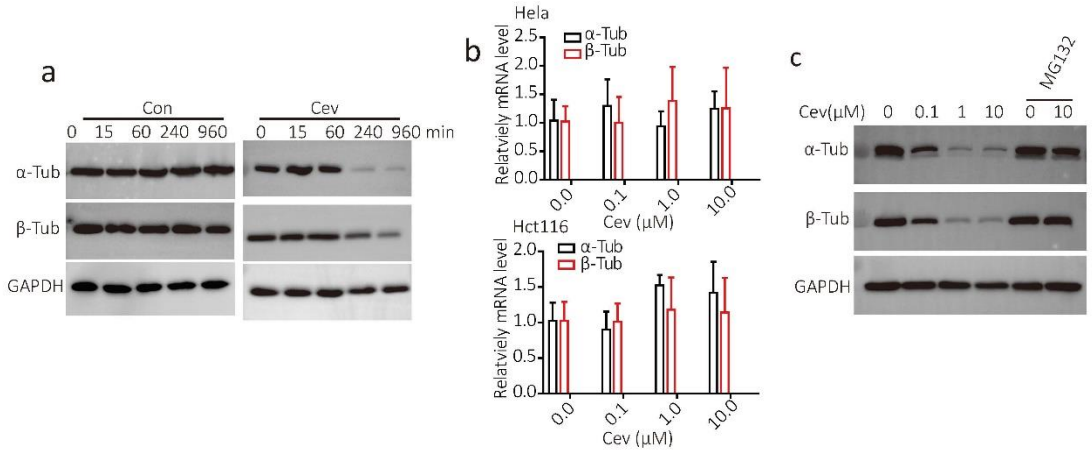

Figure S1: Cevipabulin promotes proteasome-dependent degradation of α-and β-tubulin. (**a**) HeLa cells were treated with 1 μM cevipabulin for the indicated times and then the α and β-tubulin levels were detected by immunoblotting. Results are representative of two independent experiments. (**b**) HeLa and Hct116 cells were treated with indicated concentrations of cevipabulin for 16 hours, and then mRNA levels of both *α-tubulin* and *β-tubulin* were measured by quantitative-PCR. Data were shown as means ± SD of three independent experiments. **(c**) Cells were treated with or without MG132 (20 μM) for one hour before treated with different concentrations of cevipabulin for 16 hours. Protein levels of both α- and β-tubulin were detected by immunoblotting. Results are representative of two independent experiments. Cev: cevipabulin.

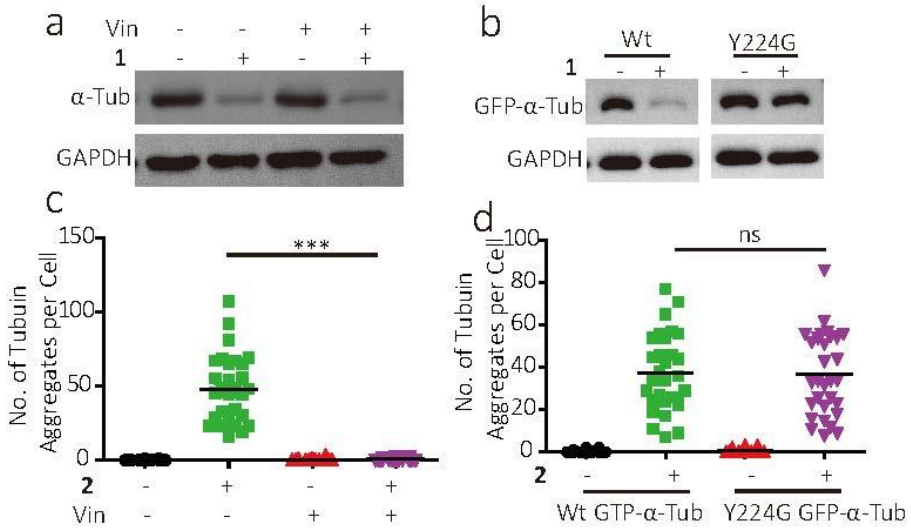

Figure S2. Compound 1 binds to vinblastine site to induce formation of irregular tubulin aggregates and compound 2 binds to the seventh site to induce tubulin degradation. (**a**) HeLa cells were treated with or without 10 μM vinblastine for 1 hour before treated with 10 μM compound 1 for 16 h and then the protein level of α-tubulin was detected by immunoblotting. Results are representative of three independent experiments. (**b**) Vectors expressing either wild type or Y224G mutant GFP-tubulin were transfected to HeLa cells. After 24 hours, cells were treated with or without 10 μM compound **1** for 16 h. Then the protein level of GFP-α-tubulin was detected by immunoblotting. Results are representative of three independent experiments. (**c**) HeLa cells were treated with or without 10 μM vinblastine for 1hour before treated with 10 μM compound **2** for another hour, and irregular tubulin aggregates were detected using immunofluorescence and the number of irregular tubulin aggregates were counted for randomly chosen 30 cells. ***p<0.0001. Results are representative of three independent experiments. (**d**) Vectors expressing either wild type or Y224G mutant GFP-α-tubulin were transfected to HeLa cells. After 24 hours, cells were treated with or without 10μM compound **2** for 1 h. Irregular tubulin aggregates were detected using immunofluorescence and the number of irregular tubulin aggregates were counted for randomly chosen 30 cells. ns: no significant difference. Results are representative of three independent experiments. Vin: vinblastine. **1**: compound **1**; **2**: compound **2**.

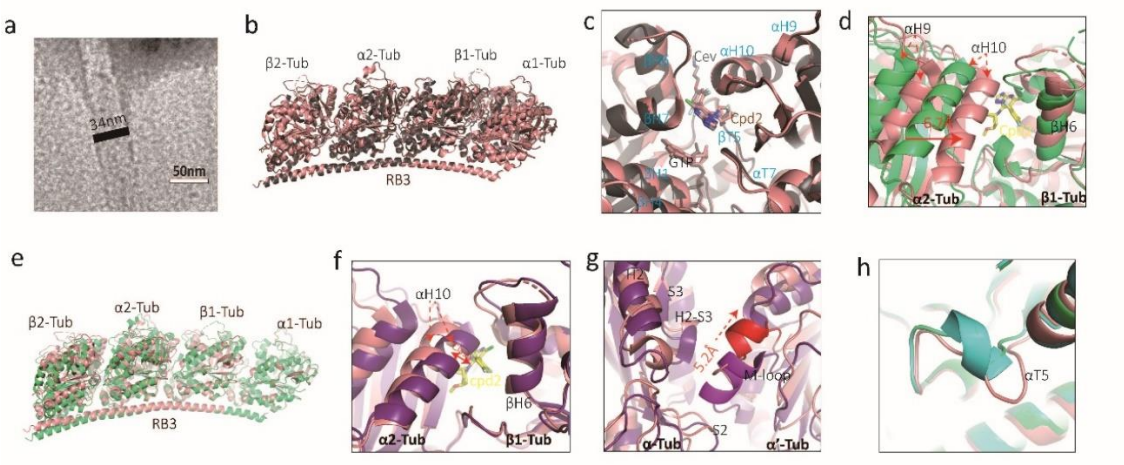

Figure S3. **Structural mechanism of cevipabulin and compound 2 induced tubulin protofilaments polymerization.** (**a**) TEM analysis of 50 μM paclitaxel treated purified tubulin. (**b**) Overview of the aligned structures of tubulin-cevipabulin complex (dark) and tubulin-compound **2** complex (salmon) (PDB code: 5NJH). (**c**) Close-up view of the cevipabulin and compound **2** binding to inter-dimer interface in the aligned complexes in (**b**). (**d**) Close-up view of the inter-dimer interface of the aligned structures of apo tubulin (green) and tubulin-compound **2** complex (dark), which are superimposed on β1-tubulin subunit. Compound **2** is shown as yellow stick. (**e**) Overview of the aligned structures in (**d**). (**f**) Close-up view of the inter-dimer interface of the aligned structures of tubulin-compound **2** complex (salmon) and the polymerized microtubule (violetpurple, PDB code: 6DPV), which are superimposed on β1-tubulin subunit. Compound **2** is shown as yellow stick. (**g**) Two tubulin-compound **2** complexes aligned to two adjacent protofilaments in polymerized microtubule structure on β1-tubulin respectively to analyze the lateral interaction. M-loop in tubulin-compound **2** complex and the polymerized microtubule structure are colored in red and purple respectively. (**h**) Tubulin-compound **2** (salmon), tubulin-vinblastine (cyan, PDB code: 5J2T) and apo tubulin (green) were aligned on α2-tubulin and the close-up view of T5 loops of α2-tubulin were shown. Cev: cevipabulin. cpd2: compound **2**.

866 **Table S1. Data collection and refinement statistics.**

867

	Tubulin-cevipabulin
Data collection	
Space group	$P2_12_12_1$
Cell dimensions	
a, *b*, *c* (Å)	104.4 160.8 174.8
α, β, γ (°)	90.0 90.0 90.0
Resolution (Å)	50.0-2.60 (2.64-2.60) *
R_{pim}	3.1 (42.2)
$I/\sigma I$	23.6 (2.0)
Completeness (%)	100 (100)
Redundancy	13.4 (13)
Refinement	
Resolution (Å)	50.0-2.61
No. reflections	83938
R_{work}/ R_{free}	20.7/25.8
No. atoms	
Protein	17464
Ligand/ion	241
Water	294
B-factors	
Protein	44
Ligand/ion	56
Water	54
R.m.s deviations	
Bond lengths (Å)	0.008
Bond angles (°)	0.789

868 *Highest resolution shell is shown in parenthesis.

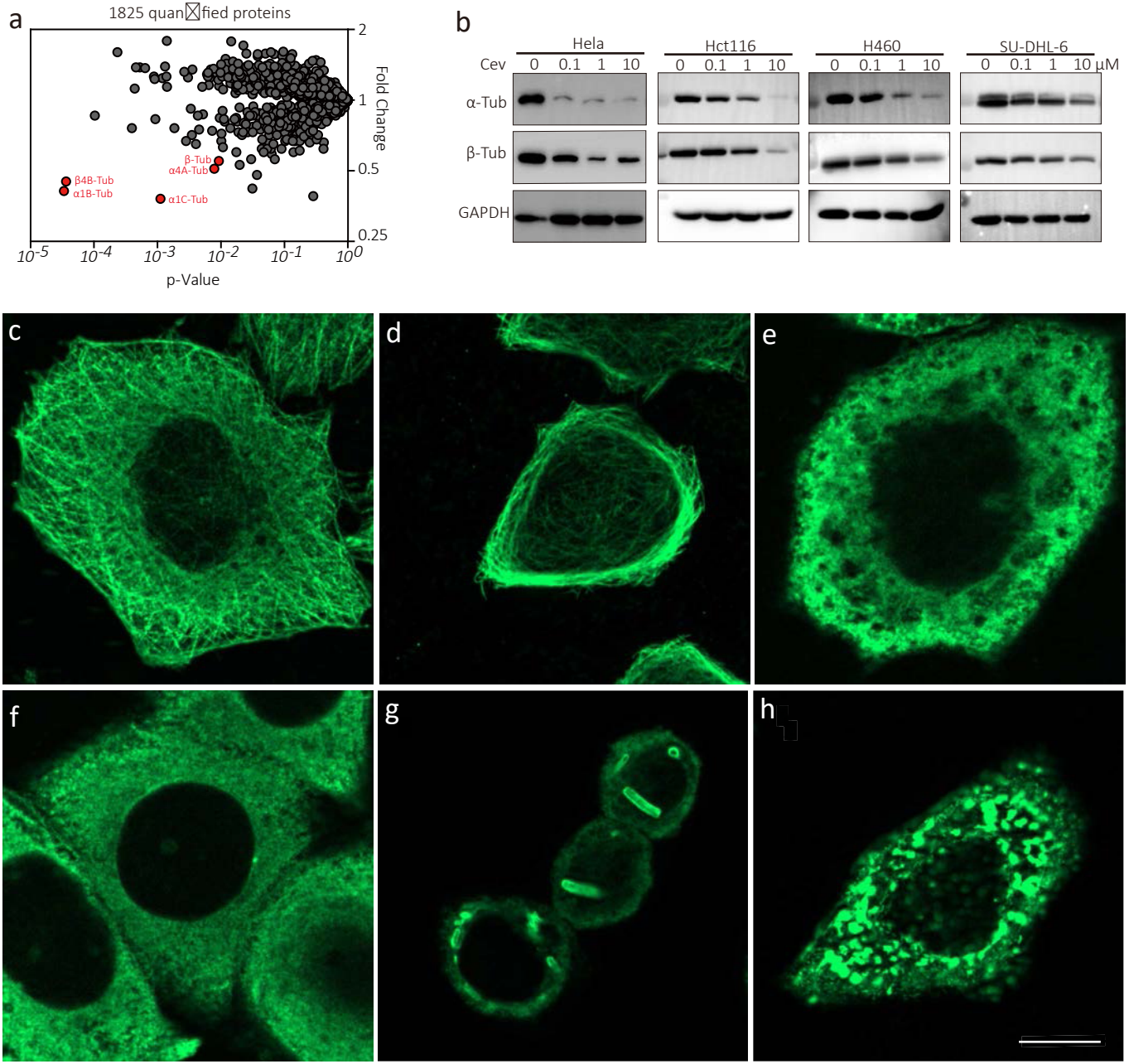
a
1825 quan☒fied proteins
Fold Change
2
1
0.5
0.25
β4B-Tub
α1B-Tub
β-Tub
α4A-Tub
α1C-Tub
10-5
10-4
10-3
10-2
10-1
100
p-Value
b
Hela
Hct116
H460
SU-DHL-6
Cev
0 0.1 1 10
0 0.1 1 10
0 0.1 1 10
0 0.1 1 10 μM
α-Tub
β-Tub
GAPDH
c
d
e
f
g
h

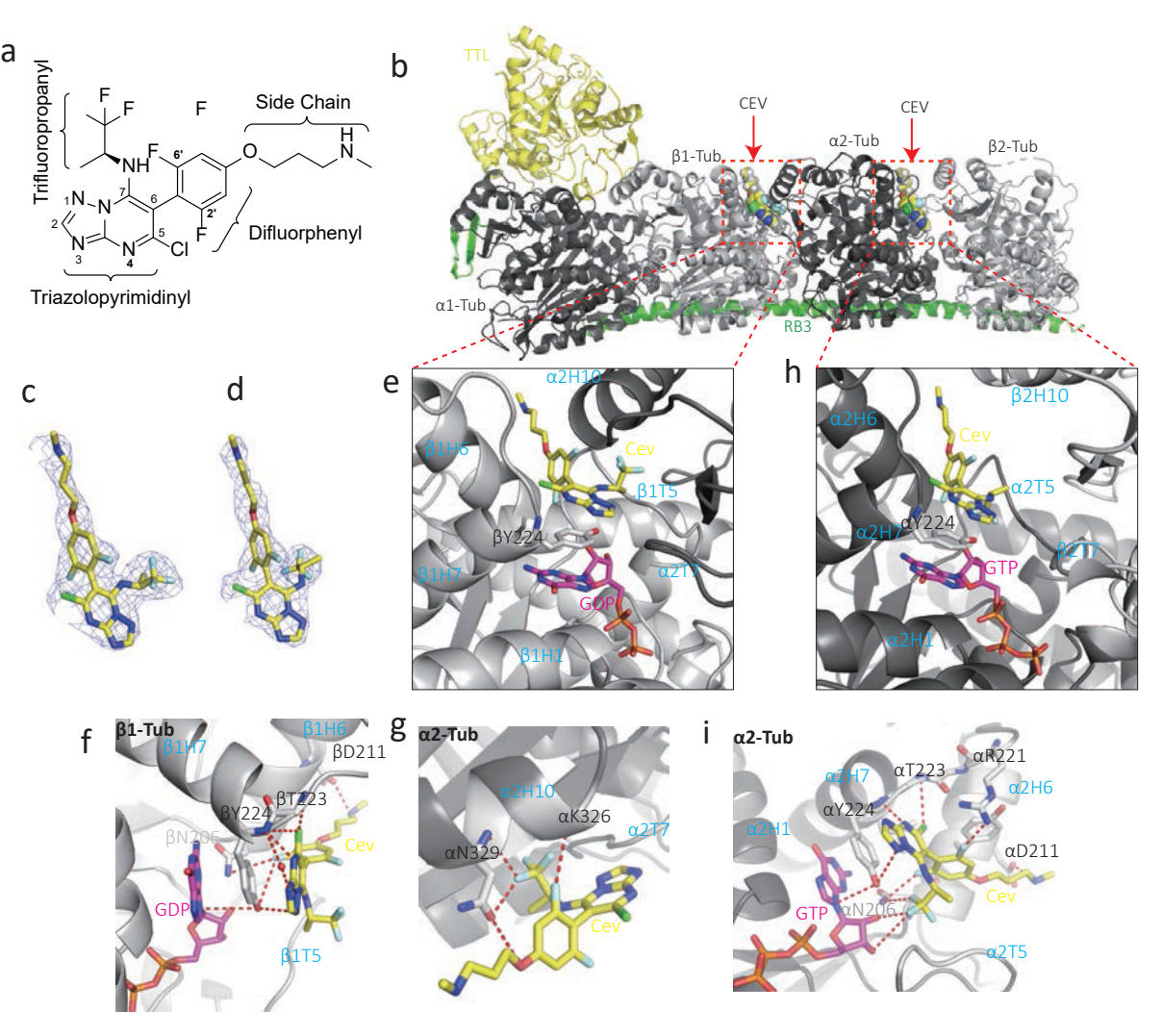
a
Trifluoropropanyl
Side Chain
Difluorphenyl
Triazolopyrimidinyl
b
TTL
CEV
CEV
β1-Tub
α2-Tub
β2-Tub
α1-Tub
RB3
c
d
e
α2H10
β1H6
Cev
β1T5
βY224
β1H7
α2T7
GDP
β1H1
h
α2H6
β2H10
Cev
α2T5
αY224
α2H7
β2T7
GTP
α2H1
f
β1-Tub
β1H7
β1H6
βD211
βY224
βT223
βN206
Cev
GDP
β1T5
g
α2-Tub
α2H10
αK326
α2T7
αN329
Cev
i
α2-Tub
αR221
α2H7
αT223
α2H6
αY224
α2H1
αD211
Cev
GTP
αN206
α2T5

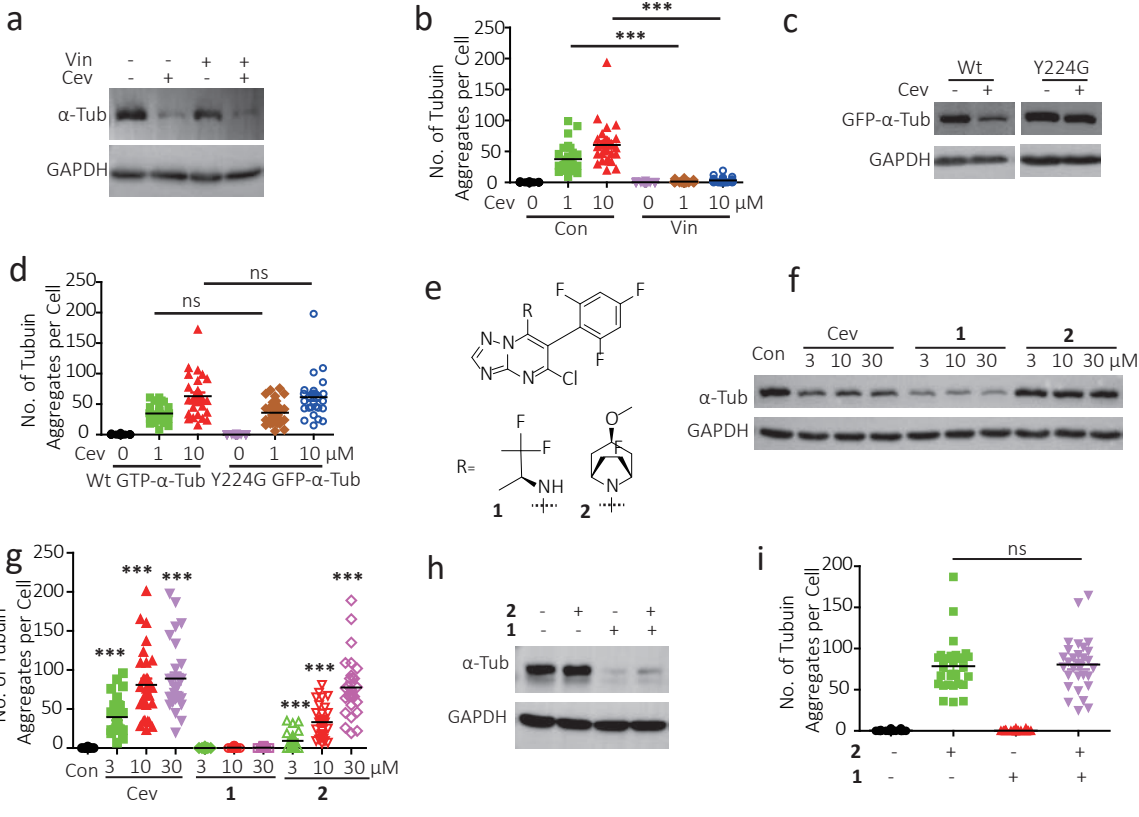
a
Vin
Cev
α-Tub
GAPDH
b
No. of Tubuin Aggregates per Cell
***
***
Cev 0 1 10 0 1 10 μM
Con
Vin
c
Wt
Y224G
Cev
GFP-α-Tub
GAPDH
d
No. of Tubuin Aggregates per Cell
ns
ns
Cev 0 1 10 0 1 10 μM
Wt GTP-α-Tub Y224G GFP-α-Tub
e
R=
1
2
f
Con
Cev
1
2
3 10 30 3 10 30 3 10 30 μM
α-Tub
GAPDH
g
No. of Tubuin Aggregates per Cell
Con 3 10 30 3 10 30 3 10 30 μM
Cev
1
2
h
2
1
α-Tub
GAPDH
i
No. of Tubuin Aggregates per Cell
ns
2
1

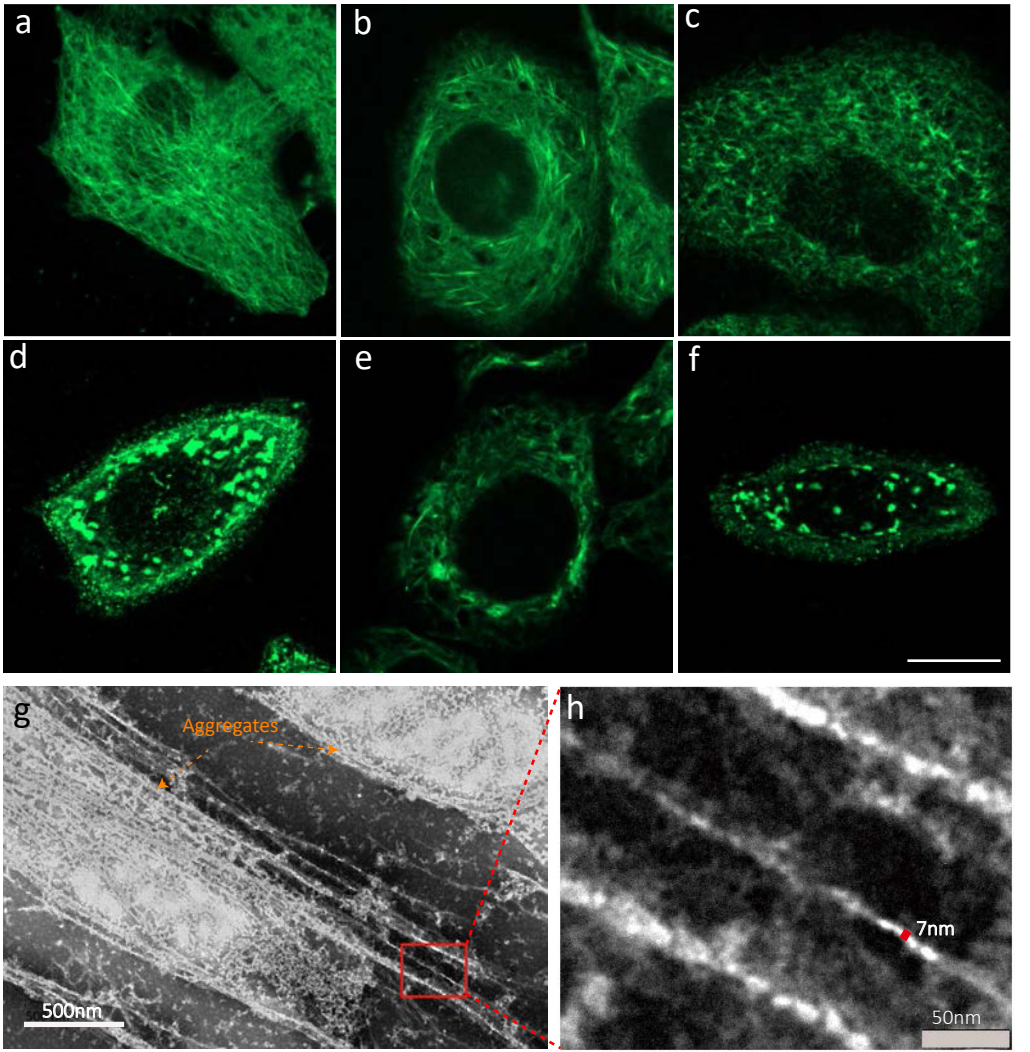
a
b
c
d
e
f
g
Aggregates
500nm
h
7nm
50nm

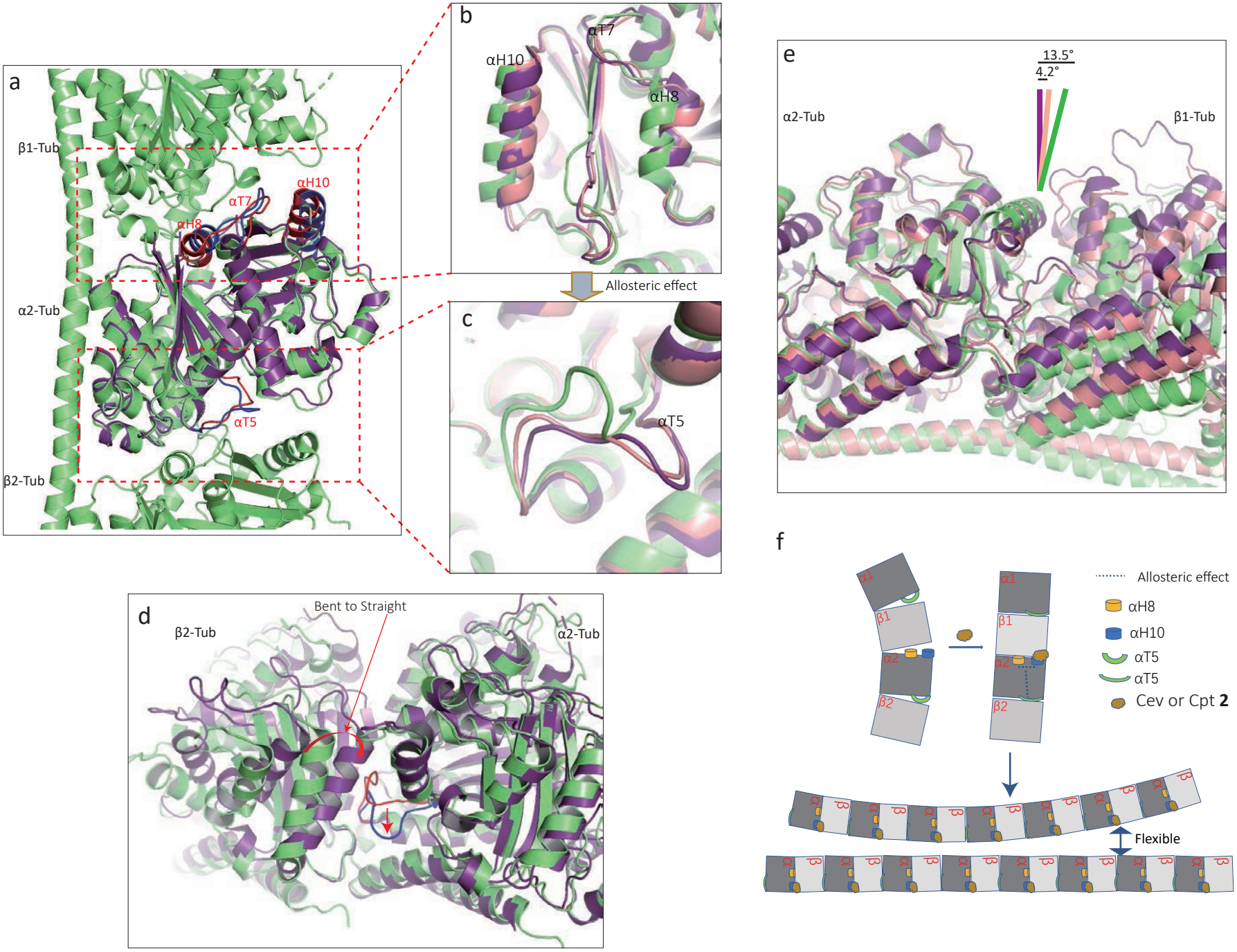
a
β1-Tub
αH10
αT7
αH8
α2-Tub
αT5
β2-Tub
b
αT7
αH10
αH8
Allosteric effect
c
αT5
d
Bent to Straight
β2-Tub
α2-Tub
e
13.5°
4.2°
α2-Tub
β1-Tub
f
α1
β1
α2
β2
Allosteric effect
αH8
αH10
αT5
αT5
Cev or Cpt 2
Flexible

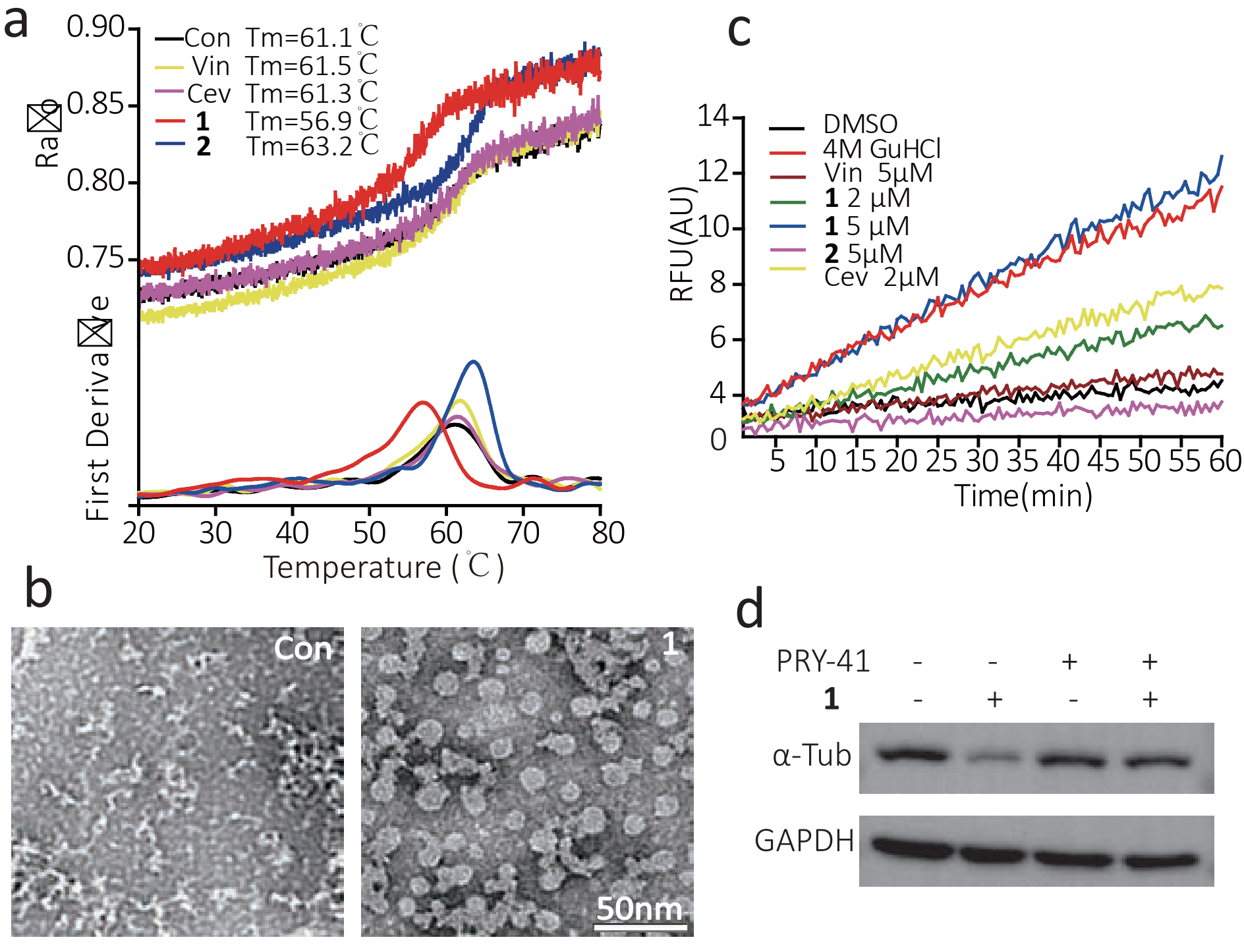
a
0.90
0.85
0.80
0.75
Con Tm=61.1℃
Vin Tm=61.5℃
Cev Tm=61.3℃
1 Tm=56.9℃
2 Tm=63.2℃
20 30 40 50 60 70 80
Temperature (℃)
c
DMSO
4M GuHCl
Vin 5μM
1 2 μM
1 5 μM
2 5μM
Cev 2μM
RFU(AU)
0 4 6 8 10 12 14
5 10 15 20 25 30 35 40 45 50 55 60
Time(min)
b
Con
1
50nm
d
PRY-41 - - + +
1 - + - +
α-Tub
GAPDH

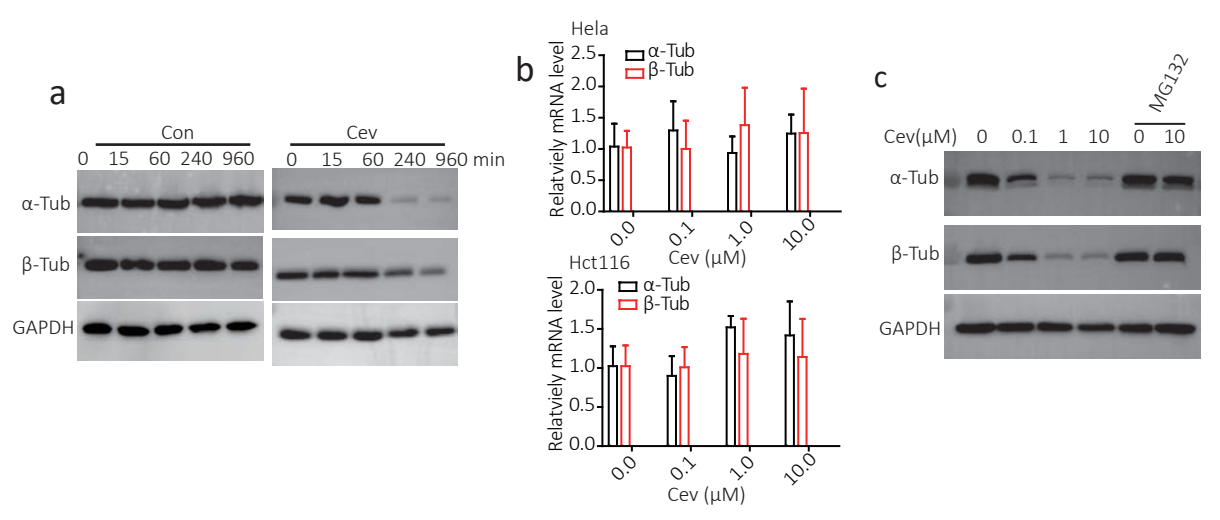
a
Con
Cev
0 15 60 240 960
0 15 60 240 960 min
α-Tub
β-Tub
GAPDH
b
Hela
Relatviely mRNA level
α-Tub
β-Tub
2.5
2.0
1.5
1.0
0.5
0.0
0.0 0.1 1.0 10.0
Cev (μM)
Hct116
Relatviely mRNA level
α-Tub
β-Tub
2.0
1.5
1.0
0.5
0.0
0.0 0.1 1.0 10.0
Cev (μM)
c
MG132
Cev(μM) 0 0.1 1 10 0 10
α-Tub
β-Tub
GAPDH

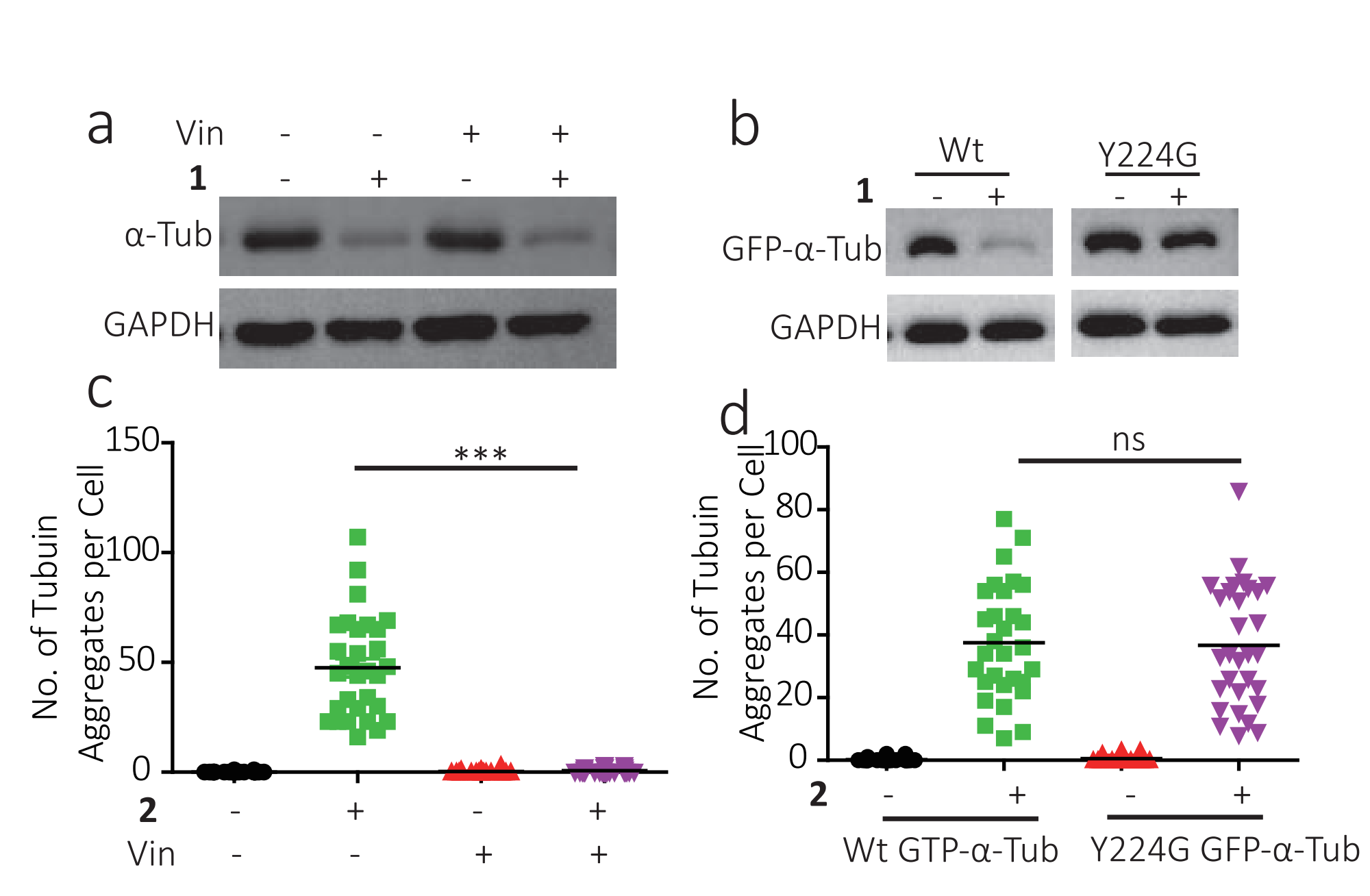
a
Vin - - + +
1 - + - +
α-Tub
GAPDH
b
Wt
Y224G
1 - + - +
GFP-α-Tub
GAPDH
c
No. of Tubuin Aggregates per Cell
150
100
50
0
***
2 - + - +
Vin - - + +
d
No. of Tubuin Aggregates per Cell
100
80
60
40
20
0
ns
2 - + - +
Wt GTP-α-Tub
Y224G GFP-α-Tub

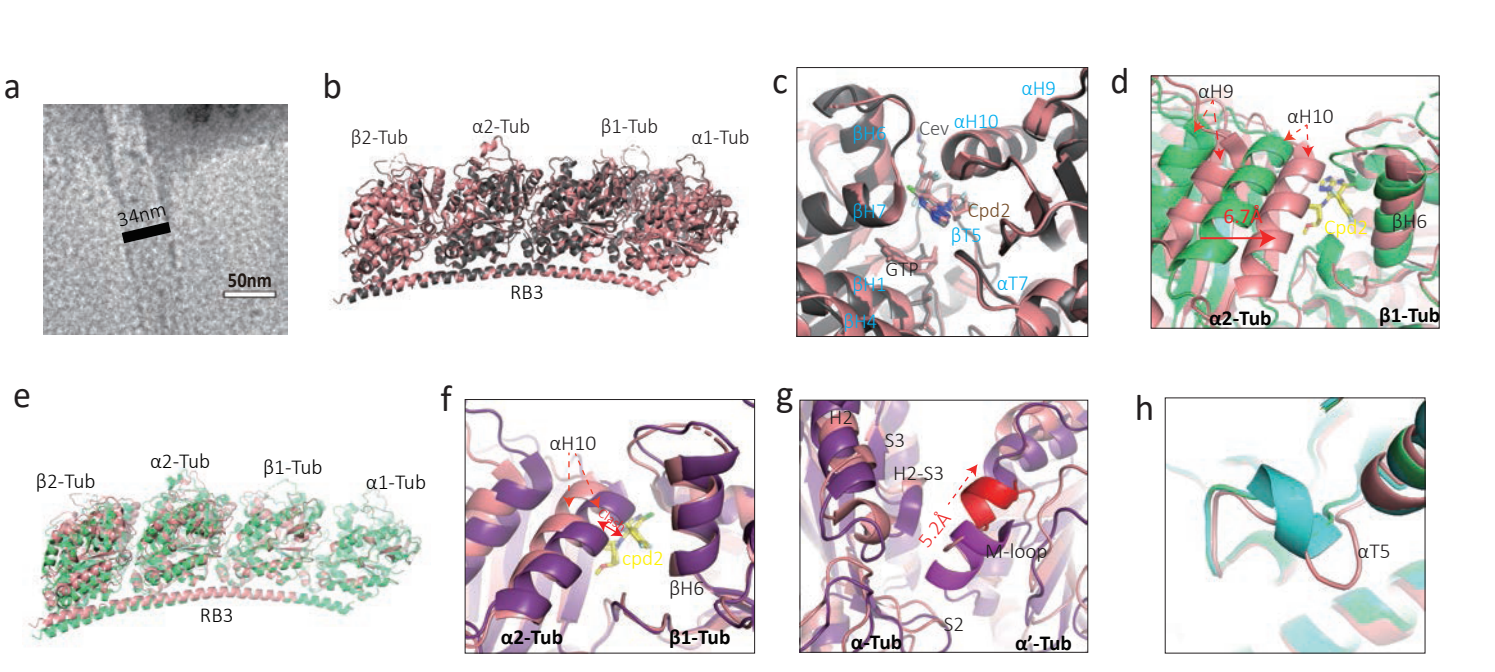
a
34nm
50nm
b
β2-Tub
α2-Tub
β1-Tub
α1-Tub
RB3
c
αH9
βH6
Cev
αH10
βH7
Cpd2
βT5
GTP
αT7
βH1
βH4
d
αH9
αH10
6.7Å
Cpd2
βH6
α2-Tub
β1-Tub
e
β2-Tub
α2-Tub
β1-Tub
α1-Tub
RB3
f
αH10
cpd2
βH6
α2-Tub
β1-Tub
g
H2
S3
H2-S3
5.2Å
M-loop
S2
α-Tub
α'-Tub
h
αT5